



This is a repository copy of *Alkali metal trihalides: MX^- ion pair or $MX-X$ complex?*

White Rose Research Online URL for this paper:

<https://eprints.whiterose.ac.uk/125313/>

Version: Accepted Version

Article:

Sun, Z., Moore, K.B., Hill, J. orcid.org/0000-0002-6457-5837 et al. (3 more authors) (2018) Alkali metal trihalides: MX^- ion pair or $MX-X$ complex? *The Journal of Physical Chemistry Part B: Condensed Matter, Materials, Surfaces, Interfaces and Biophysical*, 122 (13). pp. 3339-3353. ISSN 1089-5647

<https://doi.org/10.1021/acs.jpcb.7b10005>

Reuse

Items deposited in White Rose Research Online are protected by copyright, with all rights reserved unless indicated otherwise. They may be downloaded and/or printed for private study, or other acts as permitted by national copyright laws. The publisher or other rights holders may allow further reproduction and re-use of the full text version. This is indicated by the licence information on the White Rose Research Online record for the item.

Takedown

If you consider content in White Rose Research Online to be in breach of UK law, please notify us by emailing eprints@whiterose.ac.uk including the URL of the record and the reason for the withdrawal request.



eprints@whiterose.ac.uk
<https://eprints.whiterose.ac.uk/>

1
2
3
4
5
6
7
8
9
10
11
12
13
14
15
16
17
18
19
20
21
22

Alkali Metal Trihalides: $M^+X_3^-$ Ion Pair or $MX-X_2$ Complex?[†]

23
24
25
26
27
28
29
30
31
32
33
34
35
36
37
38
39
40
41
42
43
44
45
46
47
48
49
50
51
52
53
54
55
56
57
58
59
60

Zhi Sun,^[a] Kevin B. Moore III,^[a] J. Grant Hill,^[b] Kirk A. Peterson,^[c]

Henry F. Schaefer III*,^[a] and Roald Hoffmann*^[d]

^[a]*Center for Computational Quantum Chemistry, University of Georgia*

Athens, Georgia 30602, USA

^[b]*Department of Chemistry, University of Sheffield*

Sheffield S3 7HF, UK

^[c]*Department of Chemistry, Washington State University*

Pullman, Washington 99164, USA

^[d]*Department of Chemistry and Chemical Biology, Cornell University*

Ithaca, New York 14853-1301, USA

**E-mail: ccq@uga.edu, rh34@cornell.edu*

Abstract

The alkali metal trihalides MX_3 ($\text{M} = \text{Li, Na, K, Rb, and Cs}$; $\text{X} = \text{Cl, Br, and I}$) are systematically studied using coupled-cluster methods. Benchmarks using CCSD(T) against diatomic experimental results suggest satisfactory performance for the weighted core-valence basis sets (new basis sets for K, Rb, and Cs) selected for predicting reliable structures and harmonic vibrational frequencies. An isomer search using the B3LYP functional yields a planar, yet asymmetric T-shaped C_s structure as the global minimum for all MX_3 species. Much higher level CCSD(T) computations show a moderate to strong distortion of the X_3^- anion by the M^+ cation in the respective equilibrium geometries. Most obviously, for LiCl_3 the two Cl-Cl distances are separated by 0.786 Å. Even for CsI_3 , the structure least distorted from the M^+X_3^- model, the two I-I distances differ by 0.243 Å. It does not take much energy to distort the parent anions along an antisymmetric stretch, so this is no surprise. The normal modes of vibration of the MX_3 molecules are in better agreement with matrix isolation experiments than previous calculations. And these normal modes are revealing -- instead of the well-established antisymmetric and symmetric stretches of the “free” X_3^- anions, relatively localized and mutually-perturbed X-X and M-X stretches are calculated. The suggestion emerges that the MX_3 system may be alternatively described as an MX-X_2 complex, rather than the M^+X_3^- ion pair. This perspective is supported by bonding analyses showing low electron densities at the bond critical points and natural bond orders between the MX and X_2 moieties. The thermochemistry of fragmentations of MX_3 to $\text{MX} + \text{X}_2$ vs. $\text{M}^+ + \text{X}_3^-$ also supports the alternative viewpoint of the bonding in this class of molecules.

Introduction

There are only limited reports on the fundamental properties of alkali metal trihalides, MX_3 ($\text{M} = \text{Li}, \text{Na}, \text{K}, \text{Rb}, \text{Cs}$ and $\text{X} = \text{F}, \text{Cl}, \text{Br}, \text{I}$). Among these, the four experimental papers by Ault, Andrews, and coworkers, of these halides in a noble gas matrix at low temperatures are particularly important.¹⁻⁴

Previous theoretical studies of MX_3 virtually all focused on the X_3^- properties and assumed the validity of an M^+X_3^- ion pair model ($\text{M} = \text{Li}, \text{Na}, \text{K}, \text{Rb},$ and Cs).¹⁻⁴ The X_3^- anions have been considered as more or less “isolated”, but perturbed by the M^+ cations. A recent theoretical study of the isolated halogen clusters X_3^- by Dixon and coworkers⁵ is relevant to this situation. Early in the course of the present research we realized that Dixon’s computed harmonic vibrational frequencies (X-X-X symmetric and antisymmetric stretches) for the “free” Cl_3^- do not show satisfactory agreement with the IR/Raman frequencies of MCl_3 ($\text{M} = \text{Li}, \text{Na}, \text{K}, \text{Rb},$ and Cs) from the argon matrix experiments performed by Ault and Andrews.³ Specifically, we note significant differences (up to 114 cm^{-1} , $\sim 30\%$) between the theoretical X_3^- and experimental MX_3 vibrational frequencies. It is thus uncertain if quantitative comparisons can be made between MX_3 and X_3^- . This leads to the question: is the perturbation due to an alkali cation strong enough to substantially change the electronic structures of the X_3^- and lead to significant modifications of these anions, in terms of structures, vibrational frequencies, and bonding?

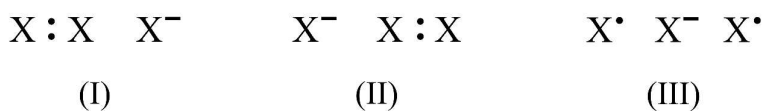
The structures and frequencies of some MX_3 species in the solid state are known,^{6,7} providing indications that the X_3^- moiety could be substantially altered by the presence of M^+ . Instead of the well-established symmetric and antisymmetric stretches^{3,5} for the “free” X_3^- anions, new modes with significant metal displacements may be involved in the MX_3 vibrations. Moreover, large red-shifts (7

1
2
3 – 11%, about 20 – 60 cm^{-1} , see Table S1 in the SI) from gas phase to argon matrices are highlighted
4
5 by Jacox⁸ for the ground state vibrational fundamentals of diatomic alkali metal halides (MX, M = Li,
6
7 Na, K, Rb, Cs and X = F, Cl, Br, I). Similar red-shifts can be also observed for the small MCl species
8
9 involved in the experimental Ault and Andrews study of MCl_3 in argon (see Table S1 in SI).³ If such
10
11 red-shifts carry over to the MX_3 species, it would impose challenges to achieving good agreement for
12
13 the vibrational frequencies between gas-phase theoretical computations⁵ and the argon matrix
14
15 experiments.¹⁻⁴ And the solid state compounds are bound to differ as well.
16
17
18
19

20
21 The solid state and noble gas matrix perturbations we just mentioned are indicative of a more
22
23 general truth: Even if we limit ourselves to an MX_3 stoichiometry, with M an alkali metal, the
24
25 richness of experimental chemistry provides us with a good number of realizations of this formula.
26
27 These include M^+ and X_3^- noninteracting in the gas phase, MX_3 molecules in a collisionless
28
29 molecular beam, MX_3 in a noble gas matrix, in solvents of varying polarity, in solids, at surfaces and
30
31 interfaces. This is hardly an exhaustive list of chemical and physical settings. Each situation will
32
33 have a different (slightly, significantly) vibrational spectrum for MX_3 . And an associated temperature.
34
35 The studies we present here are, strictly speaking, for isolated MX_3 molecules, at $T \rightarrow 0$ K.
36
37
38
39

40 For the purpose of comparison, let us review the studies of “free” trihalide anions (X_3^- , X = F, Cl,
41
42 Br, and I). These have been widely explored by both experiment and theory, in the gas phase,^{9, 10}
43
44 solution,^{11, 12} and solid state.^{13, 14} Those species have been well characterized by IR and Raman
45
46 spectra,^{3, 6, 15-17} and some gas phase thermochemistry of the X_3^- species has been reported.^{9, 10, 18, 19} In
47
48 regard to previous theoretical research, a significant focus has been the interpretation of X_3^-
49
50 electronic structure and bonding. Basically, all X_3^- species have been described as either (1) a
51
52 4-electron 3-center (4e-3c)²⁰⁻²⁴ hypervalent bonding system using the Rundle–Pimentel model,^{25, 26}
53
54
55
56
57
58
59
60

or (2) a donor-acceptor interacting system between two closed-shell fragments X_2 and X^- , (bonding types I and II in Scheme 1). Insights from molecular orbital (MO) theory are particularly relevant in this regard.^{20, 21} Hiberty and coworkers^{22, 23} employed valence-bond theory to propose another three-electron bonding type (bonding type III in Scheme 1) as an important contributor to the electronic structure of F_3^- . This special bonding character of F_3^- has been used to discuss its exceptional multireference²⁷ and symmetry-breaking²⁸ challenges, as well as its peculiar preference of the energetically disfavored dissociation channel into F_2^- and $F\cdot$ at high collision energies.¹⁸



Scheme 1. General bonding types proposed for the 4-electron 3-center hypervalent X_3^- (bonding types I and II for Cl_3^- , Br_3^- , and I_3^- ; types I, II, and III for F_3^-) systems.

Direct theoretical studies of MX_3 species have been generally limited to the fluoride systems.²⁹⁻³¹ The structures, vibrational frequencies, and dissociation energies of MF_3 ($M = Na, K, Rb,$ and Cs) were systematically studied by Tozer and Sosa²⁹ as early as 1997 using Hartree-Fock, MP2, QCISD, BLYP, and B3LYP methods. The results were found to be heavily dependent on the identity of the metals, as well as the theoretical methods applied. The method-dependence emerged in locating the true minima and corresponding vibrational frequencies, with only the B3LYP functional predicting the metal-dependent minima (Na : C_s isomer; $K, Rb,$ and Cs : C_{2v} isomer, see Figure 1) inferred from the IR/Raman spectra by Andrews and coworkers.^{32, 33} The C_{2v} isomers for KF_3 and CsF_3 were more recently (2015) studied using CCSD(T)/def2-TZVPP computations by Riedel and coworkers.³¹ The MF_3 ($M = Li, Na,$ and K) species were also studied in 2015 using the CCSD(T)/6-311+G(3df) method by Getmanskii *et al.*³⁰

Minima for all three isomers sketched in Figure 1 were located for all three fluoride species, except that the asymmetric T-shaped minimum was not found for KF_3 . The global minima for LiF_3 and NaF_3 were found to be the asymmetric and symmetric T-shaped structures, respectively. However, a tiny $0.16 \text{ kcal mol}^{-1}$ (ZPVE corrected) energy difference between the two T-shaped NaF_3 structures introduces additional uncertainties. The general preference of the C_{2v} global minimum for MF_3 could originate from the special electronic structure of F_3^- discussed above (see Scheme 1). Since the heavier X_3^- anions do not possess this unique F_3^- electronic structure, it is unclear if such structural preferences also occur for other alkali metal trihalides, MX_3 ($\text{X} = \text{Cl}, \text{Br}, \text{and I}$).

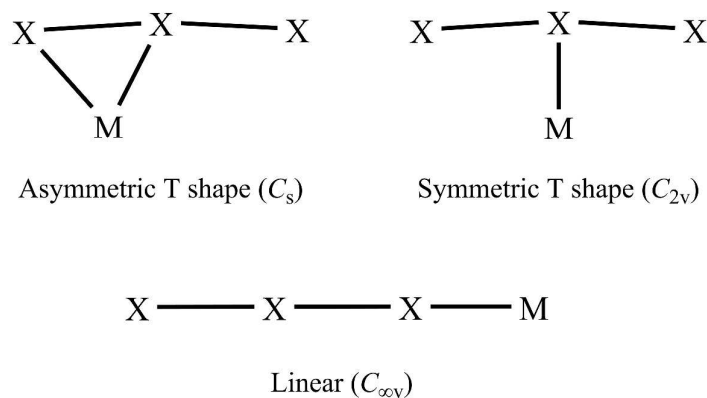


Figure 1. Structures of MF_3 ($\text{M} = \text{Li}, \text{Na}, \text{K}, \text{Rb}, \text{and Cs}$) reported in the literature.²⁹⁻³¹

There are limited theoretical and experimental results for the heavier halides MX_3 ($\text{X} = \text{Cl}, \text{Br}, \text{and I}$), and it would be beneficial to probe the latter species with rigorous computations. The present study does this, and aims to offer some answers to the following questions:

(1) Why is the agreement between theoretical⁵ X_3^- and experimental³ MX_3 vibrational frequencies relatively unsatisfactory?

(2) Could the metal-dependent global minima found^{29, 30} for MF_3 also occur for MCl_3 , MBr_3 , and

1
2
3
4 MI₃?

5
6 (3) What are the differences between X₃⁻ and MX₃ in terms of structures, vibrational modes and
7
8 frequencies, bonding characters, and thermochemistry?
9

10 (4) Finally, the title question, not anticipated, but one that arose quite naturally as we progressed:
11
12 should the alkali metal trihalides be described as ion pairs between M⁺ and X₃⁻ or as complexes
13
14 between MX and X₂?
15
16
17
18
19

20 **Theoretical Methods**

21
22
23 An isomer search for the MX₃ global minima was conducted by optimizing various prospective
24
25 structures using the B3LYP3 functional³⁴⁻³⁶ implemented in MOLPRO 2010.1.^{37, 38} This particular
26
27 version of the B3LYP functional utilizes the standard VWN3 local correlation energy parameters.³⁴
28
29 For these computations, the SCF energies and densities were both converged to 10⁻¹⁰, and the RMS
30
31 force was converged to 10⁻⁸ Hartree Bohr⁻¹. Stationary points obtained from these optimizations were
32
33 classified by their harmonic vibrational frequencies, obtained via finite differences of analytic energy
34
35 gradients. The following standard correlation consistent valence basis sets (AVTZ for simplicity)
36
37 were used in the DFT computations:
38
39
40
41

42 Li, Na: cc-pVTZ³⁹

43 K, Rb, Cs: cc-pVTZ-PP⁴⁰

44
45 Cl: aug-cc-pVTZ⁴¹

46
47 Br, I: aug-cc-pVTZ-PP⁴²

48
49
50
51
52 The equilibrium geometries, harmonic vibrational frequencies, and dissociation energies (*D*₀) of
53
54 MX₃ global minima were subsequently obtained (with new and different core-correlated basis sets)
55
56
57

1
2
3 using coupled cluster theory with single, double, and perturbative triple excitations [CCSD(T)],⁴³⁻⁴⁶
4 as implemented in CFOUR 2.0.^{47, 48} The restricted Hartree-Fock (RHF) method was used throughout,
5
6 as all the species of interest are closed-shell. For all CCSD(T) computations, the SCF densities, CC
7
8 amplitudes, and Lambda coefficients are converged to 10^{-10} . The RMS force of the geometries was
9
10 converged to 10^{-8} Hartree Bohr⁻¹. The gradients were obtained via analytic first derivatives of the
11
12 CCSD(T) energy, and the frequencies were obtained by finite differences of these gradients. Listed
13
14 below is a new group of weighted core-valence basis sets (AWCVTZ for simplicity) that was used
15
16 for the CCSD(T) computations:
17
18
19
20
21

22
23 Li, Na: cc-pwCVTZ³⁹

24
25 K, Rb, Cs: cc-pwCVTZ-PP⁴⁰

26
27 Cl: aug-cc-pwCVTZ^{41, 49}

28
29 Br, I: aug-cc-pwCVTZ-PP^{50, 51}

30
31
32 These are correlation consistent (cc), polarized (p), weighted core-valence (wCV), triple-zeta
33
34 (TZ) basis sets. Each halogen atom (Cl, Br, I) basis set is augmented with additional diffuse basis
35
36 functions to describe potential anionic character. All electrons of the Li, Na, and Cl atoms were
37
38 correlated in the CCSD(T) computations. For K, Rb, Cs, Br, and I, deep inner electrons were treated
39
40 by effective core potentials (described below). This method was chosen because the traditional
41
42 frozen-core approximation yielded several errors in the optimized structures and harmonic
43
44 vibrational frequencies for certain species (e.g. KCl₃). These issues appear to stem from systems
45
46 having correlated and uncorrelated molecular orbitals with nearly degenerate energies. Further
47
48 wavefunction diagnostics provided in the SI demonstrate that our chosen single-reference CCSD(T)
49
50 methods should be reliable. All energy and property computations were performed using the
51
52
53
54
55
56
57
58
59
60

1
2
3
4 CCSD(T)/AWCVTZ structures.

5
6 For both the B3LYP and CCSD(T) computations, we employ the multi-electron fit, fully
7
8 relativistic Köln/Stuttgart effective core-potentials (ECPs) to model the inner core electrons of the
9
10 atoms below the 3rd-row [ECP10MDF (K and Br): 10 electrons ($1s^2 2s^2 2p^6$); ECP28MDF (Rb and I):
11
12 28 electrons ($1s^2 2s^2 2p^6 3s^2 3p^6 3d^{10}$); and ECP46MDF (Cs): 46 electrons
13
14 ($1s^2 2s^2 2p^6 3s^2 3p^6 4s^2 3d^{10} 4p^6 4d^{10}$).⁵² For the atoms treated by an ECP, the corresponding -PP basis
15
16 sets are used. Since the cc-pVTZ-PP and cc-pwCVTZ-PP basis sets for K, Rb, and Cs are not yet
17
18 available in the literature, we have provided them in the Supporting Information (SI). These basis
19
20 sets are specifically matched to the ECPs mentioned above and have the following number of
21
22 primitives and contracted functions at the cc-pVTZ-PP level: K, (11s10p6d1f)/[5s4p3d1f]; Rb,
23
24 (11s9p5d1f)/[5s4p3d1f]; Cs, (11s9p6d4f)/[5s4p3d2f]. In all cases linear dependency issues were
25
26 avoided by constraining the optimizations such that the ratio between successive functions in a given
27
28 angular symmetry was greater than or equal to 1.6. The problem of correlating functions in
29
30 ECP-based calculations recovering less correlation energy than in all-electron calculations^{53, 54} was
31
32 circumvented by uncontracting an extra s-type correlating function, as in previous work.^{54, 55} The
33
34 cc-pwCVTZ-PP basis sets for these elements add 2s2p2d1f sets of functions that have been
35
36 optimized using the well-established strategy for weighted core-valence basis sets.⁴⁹ To keep
37
38 discussions throughout the main text succinct, we will refer to the mixture of these basis sets for the
39
40 B3LYP and CCSD(T) simply as AVTZ and AWCVTZ, respectively.

41
42 A bonding analysis of the optimized MX₃ species was performed using Weinhold natural bond
43
44 orbital (NBO) theory⁵⁶ and the Bader quantum theory of atoms-in-molecules (QTAIM).⁵⁷
45
46 Intermolecular hyperconjugation was quantified with the second-order energy for delocalizing
47
48
49

1
2
3 electrons from a donor orbital (L) to an acceptor orbital (NL).⁵⁸
4
5
6

$$7 \quad E(2) = q_L \frac{F(L, NL)^2}{\varepsilon_{NL} - \varepsilon_L}$$

8
9
10
11
12
13 where $F(L, NL)$ is the NBO Fock matrix element, and q_L and ε_L are the occupancy and energy of
14 orbital L, respectively. Resonance structures from natural resonance theory (NRT)⁵⁹⁻⁶¹ were obtained
15 to characterize the overall electronic structure, and types of bonding types in MX_3 . We expand this
16 picture by discussing the covalent and ionic contributions to the natural bond order. QTAIM was
17 used to locate the bond critical points to assess the electron density occurring between each atom.
18
19 The above described NBO (HF/AWCVTZ) and QTAIM (B3LYP/AVTZ) analyses were performed
20 using NBO 6.0⁵⁸ and AIMAll 16.01.09.⁶²
21
22
23
24
25
26
27
28
29
30
31
32
33
34
35
36
37
38
39
40
41
42
43
44
45
46
47
48
49
50
51
52
53
54
55
56
57
58
59
60

Results and Discussion

A systematic study of MX_3 ($\text{M} = \text{Li}, \text{Na}, \text{K}, \text{Rb}, \text{and Cs}$; $\text{X} = \text{Cl}, \text{Br}, \text{and I}$) was performed using density functional and coupled-cluster methods. In view of possible metal-dependence indicated by theoretical studies of MF_3 ($\text{M} = \text{Li}, \text{Na}, \text{K}, \text{Rb}, \text{and Cs}$),²⁹⁻³¹ several structures were considered (Figure 2) using the B3LYP functional to locate possible local minima. This was then followed by high-level coupled-cluster computations [CCSD(T) with the weighted core-valence basis sets, see Methods]. The equilibrium geometries (Table 2 and Figure 3), vibrational modes and frequencies (Tables 3-6 and Figure 5), bond analysis (Tables 7-8), thermochemistry (Table 9), and other relevant results for each species considered are reported and discussed.

Performance of the New Weighted Core-Valence Basis Sets

We wish to assess the uncertainty of the computed geometries and vibrational frequencies for the MX_3 species. In addition, the weighted core-valence basis sets for the alkali metals ($\text{K}, \text{Rb}, \text{and Cs}$, see Methods and SI) are newly developed, and no assessment of their accuracy is currently available. Since there is little experimental information on the MX_3 species, the relevant diatomic species MX and X_2 ($\text{M} = \text{Li}, \text{Na}, \text{K}, \text{Rb}, \text{Cs}$ and $\text{X} = \text{Cl}, \text{Br}, \text{I}$) are selected as a test set. Within the NIST database,⁶³ there are well-established gas phase experimental values for the equilibrium bond distances and harmonic vibrational frequencies of MX and X_2 . Within this test set, 15 ionic and 3 covalent bonds are included, and we benchmark our chosen theoretical methods against the experimental values of these species in Table 1.

TABLE 1. Benchmark of the CCSD(T)/AWCVTZ equilibrium bond lengths (in Å) and harmonic vibrational frequencies (in cm^{-1}) of MX and X_2 (M = Li, Na, K, Rb, and Cs; X = Cl, Br, and I) molecules against experimental values from the NIST tables.

Species	Equilibrium Bond Lengths				Harmonic Vibrational Frequencies		
	Computed	NIST	Deviation	Percent Error	Computed	NIST	Percent Error
LiCl	2.029	2.021	0.008	0.4%	635	643	-1.2%
NaCl	2.373	2.361	0.013	0.6%	359	366	-1.9%
KCl	2.683	2.667	0.017	0.6%	276	281	-1.8%
RbCl	2.805	2.787	0.019	0.7%	231	228	1.3%
CsCl	2.939	2.906	0.033	1.1%	210	214	-1.9%
LiBr	2.180	2.170	0.009	0.4%	553	563	-1.8%
NaBr	2.517	2.502	0.015	0.6%	293	302	-3.0%
KBr	2.838	2.821	0.018	0.6%	216	213	1.4%
RbBr	2.964	2.945	0.020	0.7%	167	169	-1.2%
CsBr	3.104	3.072	0.032	1.0%	147	150	-2.0%
LiI	2.400	2.392	0.008	0.3%	493	498	-1.0%
NaI	2.729	2.711	0.018	0.7%	254	258	-1.6%
KI	3.066	3.048	0.019	0.6%	184	187	-1.6%
RbI	3.199	3.177	0.023	0.7%	136	139	-2.2%
CsI	3.348	3.315	0.033	1.0%	117	119	-1.7%
Cl_2	2.003	1.987	0.016	0.8%	548	560	-2.1%
Br_2	2.295	2.281	0.014	0.6%	319	325	-1.8%
I_2	2.673	2.666	0.007	0.3%	217	215	0.9%
		Mean:	0.018	0.7%		Mean:	1.7%

1
2
3
4 For the equilibrium bond length, the overall mean absolute error (MAE) and mean absolute
5
6 percent error (MAPE) was found to be 0.018 Å and 0.7%, respectively. For each of the three metal
7
8 halides series (MCl, MBr, and MI), the theoretical bond lengths are all slightly longer than the
9
10 experimental values, with an increasing trend from LiX to CsX. The largest differences between
11
12 theory and experiment occur for CsX, with percent errors being 1.1%, 1.0%, and 1.0% for CsCl,
13
14 CsBr, and CsI, respectively. For the X₂ (X = Cl, Br, and I), a decreasing trend in positive deviations
15
16 (Cl₂: 0.8%, Br₂: 0.6%, and I₂: 0.3%) can be noticed.
17
18
19

20
21 For the harmonic vibrational frequencies, the overall MAPE was found to be 1.7%. From Table
22
23 1, most deviations are negative and within 2.0%. However, RbCl, KBr, and I₂ are exceptions with
24
25 positive deviations, and NaBr is the species with the highest deviation beyond 2.0% (-3.0%). No
26
27 obvious trend in percent errors can be found for the MCl and MBr series, however, the MI series
28
29 shows an increasing trend from LiI to RbI, with an exception that the percent error for CsI drops
30
31 below RbI. Consistent with the situation for bond lengths, the percent errors of the X₂ species
32
33 decrease from Cl₂ to I₂ (Cl₂: -2.1%, Br₂: -1.8%, and I₂: 0.9%).
34
35
36
37

38 In summary, the CCSD(T) method with the selected weighted core-valence basis sets predicts
39
40 reliable structures and harmonic frequencies for the relevant diatomic species MX and X₂ (M = Li,
41
42 Na, K, Rb, Cs and X = Cl, Br, I). Accordingly, the accuracy of our computed equilibrium bond
43
44 lengths and harmonic vibrational frequencies of alkali metal trihalides MX₃ should be satisfactory
45
46 for assessing the experimental conclusions of Ault, Andrews, and coworkers.³
47
48
49
50
51
52
53
54
55
56
57
58
59
60

Possible MX_3 Structures

Previous theoretical²⁹⁻³¹ and experimental studies^{32,33} have noticed that the identity of the metal (M) in the metal fluoride systems MF_3 (M = Li, Na, K, Rb, and Cs) dictates the structure of the global minimum. To investigate whether a similar metal-dependence exists for MX_3 (M = Li, Na, K, Rb, Cs and X = Cl, Br, I) species, several structures were first considered using the B3LYP/AVTZ method. The B3LYP functional was selected due to its reliable performance in the theoretical fluoride study of Tozer and Sosa²⁹ in reproducing Ault and Andrews's MF_3 experimental results.^{32,33} The isomers explored for the MX_3 (M = Li, Na, K and X = Cl, Br, I) are shown in Figure 2. The first three structures (also shown in Figure 1) were chosen because they have been previously identified as minimum-energy structures on the MF_3 potential energy surface.²⁹⁻³¹ Five additional structures (4 – 8 in Figure 2) were selected as they represent alternate symmetries, which are constrained during optimization. Also the coplanarity of all four atoms implicit in structure **1** and **2** was relaxed, effectively allowing **1** to be C_1 and **2** C_s in symmetry.

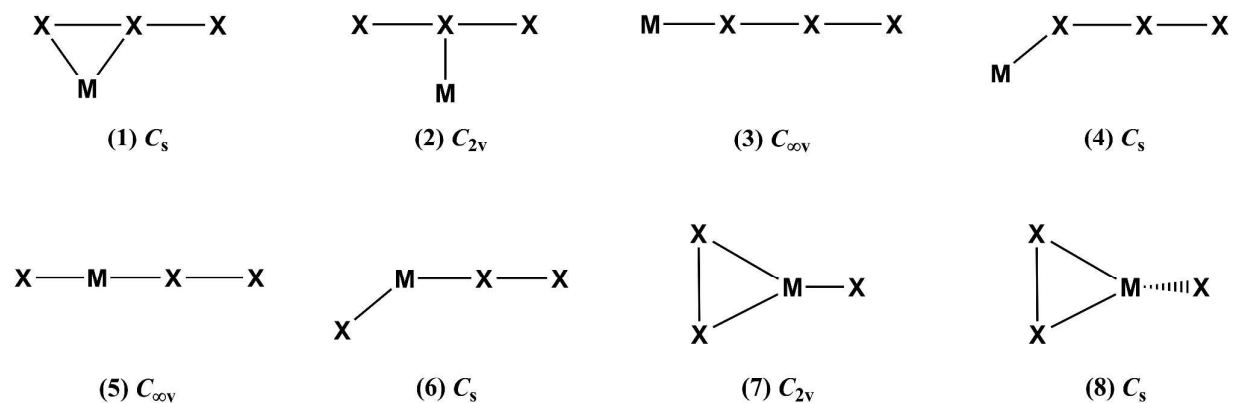


Figure 2. Possible stationary point structures explored for the MX_3 (M = Li, Na, K and X = Cl, Br, I) systems using B3LYP/AVTZ method.

1
2
3
4 In contrast to the structural variations noticed in the case of the fluoride species MF_3 ,^{29,30} results
5
6 for the other halides, the subject of this paper, are generally consistent for Li, Na, and K. For all MX_3
7
8 species, structures **1**, **2**, and **3** correspond to minima, transition states, and second-order saddle points,
9
10 respectively. The only other possible minimum was found to be the structure **7**, although it shows
11
12 some metal-dependence. The LiX_3 structures **7** were all found to be first-order saddle points with
13
14 small imaginary frequencies of $43i$, $34i$, and $22i \text{ cm}^{-1}$, for LiCl_3 , LiBr_3 , and LiI_3 , respectively. Most
15
16 NaX_3 and KX_3 structures of type **7** were predicted to be minima. However, a tiny imaginary
17
18 frequency ($5i$) and two small imaginary frequencies ($20i$ and $12i$) were predicted for NaCl_3 and KBr_3 ,
19
20 respectively. Finer integration grids might predict all real frequencies for these species, but the long
21
22 inter-fragment distance ($2.5 - 3.5 \text{ \AA}$) and the small first few frequencies (below 50 cm^{-1}) indicate that
23
24 the structure **7** is not a strongly bound minimum. Moreover, for all MX_3 species investigated,
25
26 structure **7** lies $5.9 - 15.2 \text{ kcal mol}^{-1}$ above structure **1** at the ZPVE-corrected B3LYP level.
27
28 Optimizations of structures **4**, **6**, and **8** lead to either structure **1** or **7** (see SI). Optimizations of
29
30 structure **5** separated the MX and X_2 moieties beyond 4.0 \AA .
31
32

33
34
35
36
37
38 Could structures **1** and **2** be nonplanar (as one sees in the trifluorides)? Optimizations begun in
39
40 nonplanar geometries returned uniformly to C_s and C_{2v} minima. There were two exceptions: 1. For
41
42 MCl_3 ($M=\text{Na, K, Rb, Cs}$) a noncoplanar structure derived from **2** was a stationary point that turned
43
44 out to be a transition state; the large imaginary frequency characterizing this geometry led to a
45
46 structure **1** geometry. 2. For CsBr_3 a nearly planar structure close to C_{2v} (near **2**) was a minimum,
47
48 with a low frequency (23cm^{-1}) mode leading back to structure **1**.
49
50

51
52
53
54
55
56
57
58
59
60
61
62
63
64
65
66
67
68
69
70
71
72
73
74
75
76
77
78
79
80
81
82
83
84
85
86
87
88
89
90
91
92
93
94
95
96
97
98
99
100
101
102
103
104
105
106
107
108
109
110
111
112
113
114
115
116
117
118
119
120
121
122
123
124
125
126
127
128
129
130
131
132
133
134
135
136
137
138
139
140
141
142
143
144
145
146
147
148
149
150
151
152
153
154
155
156
157
158
159
160
161
162
163
164
165
166
167
168
169
170
171
172
173
174
175
176
177
178
179
180
181
182
183
184
185
186
187
188
189
190
191
192
193
194
195
196
197
198
199
200
201
202
203
204
205
206
207
208
209
210
211
212
213
214
215
216
217
218
219
220
221
222
223
224
225
226
227
228
229
230
231
232
233
234
235
236
237
238
239
240
241
242
243
244
245
246
247
248
249
250
251
252
253
254
255
256
257
258
259
260
261
262
263
264
265
266
267
268
269
270
271
272
273
274
275
276
277
278
279
280
281
282
283
284
285
286
287
288
289
290
291
292
293
294
295
296
297
298
299
300
301
302
303
304
305
306
307
308
309
310
311
312
313
314
315
316
317
318
319
320
321
322
323
324
325
326
327
328
329
330
331
332
333
334
335
336
337
338
339
340
341
342
343
344
345
346
347
348
349
350
351
352
353
354
355
356
357
358
359
360
361
362
363
364
365
366
367
368
369
370
371
372
373
374
375
376
377
378
379
380
381
382
383
384
385
386
387
388
389
390
391
392
393
394
395
396
397
398
399
400
401
402
403
404
405
406
407
408
409
410
411
412
413
414
415
416
417
418
419
420
421
422
423
424
425
426
427
428
429
430
431
432
433
434
435
436
437
438
439
440
441
442
443
444
445
446
447
448
449
450
451
452
453
454
455
456
457
458
459
460
461
462
463
464
465
466
467
468
469
470
471
472
473
474
475
476
477
478
479
480
481
482
483
484
485
486
487
488
489
490
491
492
493
494
495
496
497
498
499
500
501
502
503
504
505
506
507
508
509
510
511
512
513
514
515
516
517
518
519
520
521
522
523
524
525
526
527
528
529
530
531
532
533
534
535
536
537
538
539
540
541
542
543
544
545
546
547
548
549
550
551
552
553
554
555
556
557
558
559
560
561
562
563
564
565
566
567
568
569
570
571
572
573
574
575
576
577
578
579
580
581
582
583
584
585
586
587
588
589
590
591
592
593
594
595
596
597
598
599
600
601
602
603
604
605
606
607
608
609
610
611
612
613
614
615
616
617
618
619
620
621
622
623
624
625
626
627
628
629
630
631
632
633
634
635
636
637
638
639
640
641
642
643
644
645
646
647
648
649
650
651
652
653
654
655
656
657
658
659
660
661
662
663
664
665
666
667
668
669
670
671
672
673
674
675
676
677
678
679
680
681
682
683
684
685
686
687
688
689
690
691
692
693
694
695
696
697
698
699
700
701
702
703
704
705
706
707
708
709
710
711
712
713
714
715
716
717
718
719
720
721
722
723
724
725
726
727
728
729
730
731
732
733
734
735
736
737
738
739
740
741
742
743
744
745
746
747
748
749
750
751
752
753
754
755
756
757
758
759
760
761
762
763
764
765
766
767
768
769
770
771
772
773
774
775
776
777
778
779
780
781
782
783
784
785
786
787
788
789
790
791
792
793
794
795
796
797
798
799
800
801
802
803
804
805
806
807
808
809
810
811
812
813
814
815
816
817
818
819
820
821
822
823
824
825
826
827
828
829
830
831
832
833
834
835
836
837
838
839
840
841
842
843
844
845
846
847
848
849
850
851
852
853
854
855
856
857
858
859
860
861
862
863
864
865
866
867
868
869
870
871
872
873
874
875
876
877
878
879
880
881
882
883
884
885
886
887
888
889
890
891
892
893
894
895
896
897
898
899
900
901
902
903
904
905
906
907
908
909
910
911
912
913
914
915
916
917
918
919
920
921
922
923
924
925
926
927
928
929
930
931
932
933
934
935
936
937
938
939
940
941
942
943
944
945
946
947
948
949
950
951
952
953
954
955
956
957
958
959
960
961
962
963
964
965
966
967
968
969
970
971
972
973
974
975
976
977
978
979
980
981
982
983
984
985
986
987
988
989
990
991
992
993
994
995
996
997
998
999
1000

Though the C_s structures are definitely preferred, the question could be asked “By how much?”
Some representative numbers for the energy difference between optimized C_s and C_{2v} structures are

1
2
3 -11.0 kcal/mol for LiCl₃, 1.1 kcal/mol for CsCl₃, 10.0 kcal/mol for LiI₃, 1.2 kcal/mol for CsI₃. For Li
4
5 species, the C_s and C_{2v} structures are clearly separated by ~10 kcal/mol. However, the CsX₃ (X = Cl
6
7 or I) have C_s and C_{2v} structures nearly degenerate in energy, consistent with their small imaginary
8
9 frequencies (55*i* and 16*i* for CsCl₃ and CsI₃, respectively) in their C_{2v} shape. This is an indication
10
11 that large alkali metals (such as Cs) tend to have less impact on the X₃⁻ than the small ones (Li, for
12
13 instance). We will explore this point further in the following sections.
14
15
16
17

18 In summary, the strong metal-dependence reported for the MF₃ (M = Li, Na, K, Rb, and Cs)^{29, 30}
19
20 species does not appear to carry over to the MX₃ (X = Cl, Br, and I) systems. In contrast to the
21
22 general preference for a C_{2v} global minimum for MF₃, our DFT computations suggest that the
23
24 asymmetric T-shaped C_s structure (structure **1** in Figure 2) is a global minimum for all MX₃ species.
25
26 This is consistent with the Ault and Andrews's experimental finding for MCl₃ (M = Li, Na, K, Rb,
27
28 and Cs).³ We only focus on the asymmetric T-shaped global minimum for the rest of the discussion.
29
30
31
32
33
34
35
36
37
38
39
40
41
42
43
44
45
46
47
48
49
50
51
52
53
54
55
56
57
58
59
60

Equilibrium Geometries for MX_3

The labels of atoms and bonds in MX_3 ($\text{M} = \text{Li}, \text{Na}, \text{K}, \text{Rb}, \text{and Cs}$; $\text{X} = \text{Cl}, \text{Br}, \text{and I}$) are shown in Figure 3, and the parameters of all equilibrium geometries are listed in Table 2. For comparison, the “free” X_3^- ($\text{X} = \text{Cl}, \text{Br}, \text{and I}$) geometries are also reported.

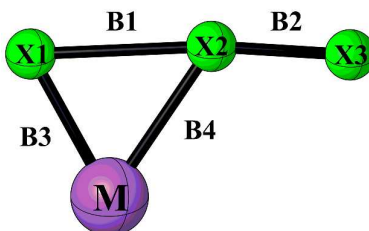


Figure 3. Labels of atoms and bonds in MX_3 ($\text{M} = \text{Li}, \text{Na}, \text{K}, \text{Rb}, \text{and Cs}$; $\text{X} = \text{Cl}, \text{Br}, \text{and I}$) used in Table 2.

For the trihalide series seen in Table 2, the Cl-Cl bond distance in the “free” Cl_3^- (D_{oh}) is predicted to be 2.313 Å at the CCSD(T)/aug-cc-pwCVTZ level. This value agrees well with the CCSD(T)/aug-cc-pV(T+d)Z result (2.314 Å) by Dixon and coworkers⁵ and the CCSD(T)/aug-cc-pVQZ result (2.313 Å) by Riedel *et al.*⁶⁴ The Br-Br bond distance in Br_3^- is predicted to be 2.571 Å at the CCSD(T)/aug-cc-pwCVTZ-PP level. This value is slightly shorter than the Br-Br distance (2.585 Å) computed at the CCSD(T)/aug-cc-pVTZ-PP level by Dixon and coworkers.⁵ Both Cl-Cl and Br-Br bond distances are also close to DFT results obtained at the MPWB1K/6-31+G(d) level of theory by Pichierri.⁶⁵ The I-I bond distance in “free” I_3^- is predicted to be 2.944 Å at the CCSD(T)/aug-cc-pwCVTZ-PP level. This value is shorter than the I-I distance (2.973 Å) computed with the CCSD(T)/aug-cc-pVTZ-PP method by Dixon and coworkers.⁵ However, our distance agrees well with the result (2.945 Å) at the CCSD(T)/aug-cc-pVTZ-PP level (all orbitals are correlated) by Braïda and Hiberty.²³ The difference in bond lengths calculated with

ostensibly the same methodology, not to speak of what would be obtained with different levels of calculation, serves in a way to set the theoretical equivalent of an error bar on a calculation.

TABLE 2. Equilibrium geometries (bond lengths in Å and angles in degrees) of MX_3 ($\text{M} = \text{Li}, \text{Na}, \text{K}, \text{Rb},$ and Cs ; $\text{X} = \text{Cl}, \text{Br}$ and I) minima (see Figure 3) optimized using the CCSD(T)/AWCVTZ method. Previously reported values are given in parentheses.

Species	B1(X1-X2)	B2(X2-X3)	B3(M-X1)	B4(M-X2)	A(X1-X2-X3)	A(X1-M-X2)
Cl_3^-	2.313 (2.314 ^a , 2.313 ^b)	2.313 (2.314 ^a , 2.313 ^b)	-	-	180.0	-
LiCl_3	2.836	2.050	2.079	2.382	169.1	78.6
NaCl_3	2.719	2.078	2.440	2.733	174.1	63.1
KCl_3	2.598	2.116	2.786	2.982	174.3	53.4
RbCl_3	2.569	2.127	2.925	3.096	174.1	50.4
CsCl_3	2.553	2.132	3.084	3.253	174.1	47.4
Br_3^-	2.571 (2.585 ^a)	2.571 (2.585 ^a)	-	-	180.0	-
LiBr_3	2.879	2.385	2.269	2.463	171.0	74.8
NaBr_3	2.817	2.410	2.629	2.809	174.0	62.3
KBr_3	2.741 (2.64 ^c)	2.441 (2.49 ^c)	2.989	3.083	173.2	53.6
RbBr_3	2.721	2.450	3.137	3.199	172.7	50.9
CsBr_3	2.702 (2.698 ^d)	2.458 (2.440 ^d)	3.312	3.344	172.0	47.9
I_3^-	2.944 (2.972 ^a , 2.945 ^e)	2.944 (2.972 ^a , 2.945 ^e)	-	-	180.0	-
LiI_3	3.229	2.769	2.504	2.664	170.2	77.3
NaI_3	3.182	2.790	2.855	3.017	173.4	65.6
KI_3	3.113	2.816	3.226	3.321	172.9	56.8
RbI_3	3.095 (3.051 ^f)	2.824 (2.833 ^f)	3.376	3.444	172.4	54.0
CsI_3	3.075 (3.03 ^g)	2.832 (2.83 ^g)	3.552	3.589	171.7	51.0

^a The CCSD(T)/aug-cc-pV(T+d)Z values from ref. 5. ^b The CCSD(T)/aug-cc-pVQZ values from ref. 64. ^c X-ray values of *Pnma* KBr_3 crystal from ref. 66. ^d X-ray values of *Pmnb* CsBr_3 crystal from ref. 67. ^e The CCSD(T)/aug-cc-pVTZ-PP values from ref. 23. ^f X-ray values of *Pnma* RbI_3 crystal from ref. 68. ^g X-ray values of CsI_3 crystal from refs. 69 and 70.

There are to date limited reports of any type for the MX_3 ($\text{X} = \text{Cl}, \text{Br},$ and I) structures in the gas phase or in matrices. Hence we are drawn to some solid state results. And here we need to insert an anticipation of what Table 2 holds, which can be summarized as a variable asymmetrization of the

trihalide moiety of MX_3 , in the asymmetric environment the trihalide faces in a C_s geometry.

Such asymmetrization is a sign of the relatively small energy involved in changing the B1 and B2 bond lengths from equality in X_3^- itself, no cation present, along an antisymmetric stretching coordinate. Experimentally, the evidence for this is the beautiful Bürgi and Dunitz diagram (a plot of B1 vs B2) for all the triiodide structures in the Cambridge Structural Database (CSD⁷¹) in 2003, by Svensson and Kloo.⁷² We have regenerated this plot in Figure 4, The impetus for a structure to move from the 45° line (B1=B2) is, of course, the asymmetry of the counter-cation in the structure, or the crystal packing. Whichever it is, the hyperbola we see is *prima facie* evidence of an energetically easy excursion along a very specific potential energy surface in which $\text{B1} \neq \text{B2}$. A similar diagram for tribromide structures may be found in Robertson et al.¹⁴

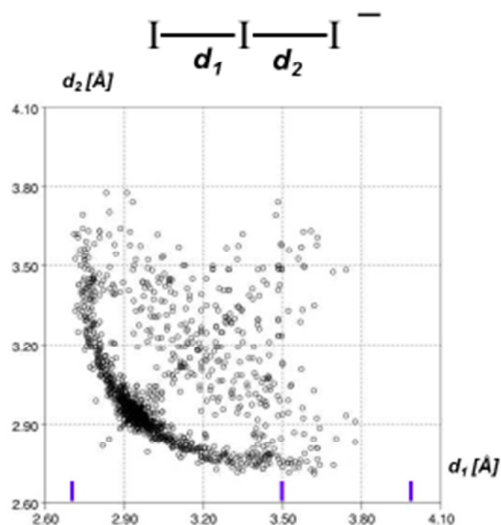


Figure 4. A plot of the two distances, d_1 and d_2 (corresponding to our B1 and B2) in the triiodide structures in the Cambridge Structural Database.

We can simulate the energetics involved theoretically by fixing $2.67 \text{ \AA} < \text{B1} < 2.94 \text{ \AA}$ (the limits are its values in I_2 and I_3^-), and allowing B2 to vary. The resulting plot (in the SI) reproduces the hyperbola pretty well, and shows that it takes 4.8 kcal/mol for I_3^- to move from $\text{B1} = 2.67 \text{ \AA}$, $\text{B2} =$

1
2
3 3.07 Å to B1 = B2 = 2.94 Å.
4
5

6 Returning to specifically MX_3 structures, with the M of this study, we do find some in the
7 literature. In these, even if the stoichiometry is MX_3 , one does not have a molecular crystal of MX_3
8 entities well-separated from other such molecules; instead there are arrangements of varying
9 complexity of X_3 anions of varying asymmetry, and the M cations. The structures resolved in
10 previous experimental studies at least in part to give an idea of their complexity.
11
12
13
14
15
16
17

18 The structures observed fall into three groups: (1) MX_3 solid state structures; (2) $\text{MX}_3 \cdot Z$, where
19 one or more Z molecules accompany the metal halide in the solid state structure; (3) extended
20 structures associated with high pressure environments, often theoretical.
21
22
23
24

25 In group 1 we have structures of CsBr_3 , RbI_3 and CsI_3 (the latter done independently by two
26 groups, and also at -160°C).^{67, 68, 70, 73} In each case, the coordination environment of the trihalide is
27 far from simple – for instance in CsBr_3 the tribromide group has no less than 8 different Cs^+ ions
28 coordinated to it, at 3.52-4.02 Å. And that coordination environment is very, very different from that
29 we calculate for our isolated MX_3 molecules. Nevertheless, the observed asymmetries of the
30 trihalides in these structures quite remarkably resemble those calculated by us for isolated molecules.
31
32
33
34
35
36
37
38
39
40 In the crystal structure of CsBr_3 in *Pmnb* space group,⁶⁷ the experimental Br-Br bond length pair was
41 reported to be 2.698/2.440 Å, which agrees well with the values 2.702/2.458 Å reported in the
42 present research. The I-I bond length pairs in the RbI_3 ⁶⁸ and CsI_3 ^{69, 70} crystal structures were reported
43 to be 3.051/2.833 and 3.04/2.84 Å (some variation among the crystal structures), respectively, and
44 the two sets of values are close to the corresponding 3.095/2.824 and 3.075/2.832 Å obtained at the
45 CCSD(T)/AWCVTZ level in this work. A theoretical study of the CsI_3 crystal finds 3.01/2.90 Å.⁷⁴
46
47
48
49
50
51
52
53
54

55 The second group – MX_3 associated with other molecules – is a rich one. Here are three
56
57
58
59
60

1
2
3 examples of many: $\text{KI}_3 \cdot \text{H}_2\text{O}$, $\text{KI} \cdot \text{KI}_3 \cdot 6(\text{N-methyacetamide})$, $\text{Cs}_2\text{I}_8 = \text{Cs}_2 \cdot (\text{I}_3)_2 \cdot \text{I}_2$.⁷⁵⁻⁷⁷ Naturally, the
4
5 triiodide environments are still more complex in these compounds. Remarkably the triiodide in
6
7 $\text{KI}_3 \cdot \text{H}_2\text{O}$ is nearly symmetrical, I-I 2.925/2.935 Å, the asymmetry calculated by us is 2.816/3.182 Å.
8
9 The trihalides in Cs_2I_8 are closer to our molecular asymmetry, at 2.84/3.00 Å. One has to draw an
10
11 imaginary line somewhere in listing compounds in this class, as the structures quickly shade over to
12
13 the multitudinous class of polyiodides, in which trihalides interact weakly or strongly with iodide
14
15 ions and I_2 molecules.⁷²
16
17
18
19

20
21 The high pressure structures, the third group, are a relatively new phenomenon, one with which
22
23 one of us (RH) is much involved. Under extreme conditions of elevated pressure new stoichiometries
24
25 emerge, simply not there at 1 atm. Calculations often precede syntheses in this playground; actual
26
27 observation of predicted phases is relatively rare. In the two cases we mention, NaCl_3 and KCl_3 , one
28
29 actually has seen the compositions in experiment. In the NaCl_3 crystal structure ($Pm\bar{3}n$ space group)
30
31 at high pressure (200 GPa),⁷⁸ the shortest Cl-Cl and Na-Cl bond distances were recently reported to
32
33 be 2.06 and 2.30 Å. These two distances are not far from to 2.078 and 2.440 Å (B2 and B3 in Figure
34
35 3 and Table 2) at the CCSD(T)/AWCVTZ level in this work, respectively. The Br-Br bond length
36
37 pair in KBr_3 was reported in 2017 to be 2.64/2.49 and 2.90/2.51 Å in $Pnma$ (4 GPa) and $P\bar{3}c1$ (15
38
39 GPa) space groups, respectively.⁶⁶ These distances may be compared to our theoretical values
40
41 2.741/2.441 Å (Table 2) at the CCSD(T)/AWCVTZ level. In general, it may not be fair to compare
42
43 distances in a calculated compressed crystal with our isolated molecule values at $P = 1$ atm.
44
45
46
47
48
49

50
51 Returning to our computational results, summarized in Table 2, in all MX_3 structures, a clear
52
53 decreasing and increasing trend can be observed in the change of B1 (X1-X2) and B2 (X2-X3) bond
54
55 lengths from Li to Cs, respectively. In other words, the bonds B1 and B2 tend to converge at CsX_3
56
57
58
59
60

1
2
3 with a distorted structure compared to the “free” X_3^- (Cl-Cl: 2.313 Å; Br-Br: 2.571 Å; I-I: 2.944 Å,
4 Table 2), implying a decreasing interaction of M^+ with X_3^- , probably due to the increasing
5 metal-halogen distance from Li^+ to Cs^+ . Moreover, the Br_3^- and I_3^- are less distorted than Cl_3^- by the
6 same alkali metal, in terms of the imbalance of bond pair B1/B2 in Table 2. Both B3 (X1-M) and B4
7 (X2-M) keep increasing because of the enlarged atomic size from Li to Cs, and the bond pair B3/B4
8 distances become more similar from LiX_3 to CsX_3 . Particularly, the B3 and B4 distances in $CsBr_3$
9 and CsI_3 are almost equal with a $\Delta(B3-B4)$ of only about 0.03-0.04 Å, whereas it is relatively large
10 for $CsCl_3$ (~0.17 Å).
11
12
13
14
15
16
17
18
19
20
21
22

23 We already mentioned the $MX \cdot X_2$ perspective, which emerges in the next section; the similarity
24 of B2 and B3 distances brings to mind still another viewpoint, an organometallic one: it suggests an
25 M^+ ion π -bonding to just one pair of atoms in a trihalide anion.
26
27
28
29

30 Most importantly, the internuclear distance between M and atom X3 (Figure 3) is always long
31 (mostly beyond 4.0 Å, with the exception of Li-Cl3 being 3.901 Å). Hence no strong interaction
32 between the alkali metal and this particular halogen atom X3 is seen. This is consistent with the
33 observation that the MX_3 (M = Li, Na, K, Rb, Cs and X = Cl, Br, I) species all possess an
34 asymmetric T-shaped C_s equilibrium structure, instead of a symmetric C_{2v} structure (Figure 1), such
35 that is seen for most MF_3 species.²⁹⁻³¹ Such a different preference of symmetry between MF_3 and
36 MX_3 is largely dictated by the different electronic structures of the two, which has been discussed in
37 the Introduction (see also Scheme 1).
38
39
40
41
42
43
44
45
46
47
48
49

50 For the angle $A(X1-X2-X3)$ in Table 2, a ~6–10° deviation from linear X_3^- is noticed for all MX_3
51 series. The LiX_3 always possess the most bent $A(X1-X2-X3)$ angle, which is about 10° from linearity
52 and distinct from those of NaX_3 by 3°–5°. The $A(X1-X2-X3)$ angles from NaX_3 to CsX_3 are more
53
54
55
56
57
58
59
60

1
2
3 consistent, especially for the MCl_3 . However, a slightly decreasing trend from Na to Cs can be found
4
5
6 for the MBr_3 and MI_3 series. In the Svensson and Kloo review of triiodide structures, their Fig. 10
7
8 shows small departures from triiodide linearity in hundreds of such structures. Departures from
9
10 linearity of $\sim 6\text{--}10^\circ$ are rare; indicating in still another way the strong M- X_3 bonding. In discrete
11
12 molecules, in addition, the angle $\angle(X1-M-X2)$ becomes increasingly acute due to the enlarged
13
14 atomic size from Li to Cs.
15
16

17
18 In summary, our geometrical parameters show reasonable agreement with available experiments.
19
20 For all three MX_3 series, the trend in geometrical change indicates a generally decreasing distortion
21
22 of the X_3^- structure by M^+ from Li^+ to Cs^+ . C_s (and not C_{2v}) symmetry is established for all MX_3 (X
23
24 = Cl, Br, and I). Such preference for C_s symmetry is also reflected in the MX_3 harmonic vibrational
25
26 modes and frequencies, which are discussed in the following section.
27
28
29
30
31
32

33 **Vibrational Modes and Frequencies of MX_3**

34
35 Generally, for the “free” D_{oh} X_3^- ($X = \text{Cl, Br, and I}$) anions, the antisymmetric stretch (σ_u) and
36
37 bend mode (π_u) are both IR-active, while the symmetric stretch (σ_g) is Raman-active, as shown at the
38
39 top of Figure 5. Since the MX_3 experiments necessarily contain counteranions, which distort the X_3^-
40
41 into a lower symmetry, both stretches are expected to have substantial intensity in the IR and Raman
42
43 spectra.
44
45
46
47
48
49
50
51
52
53
54
55
56
57
58
59
60

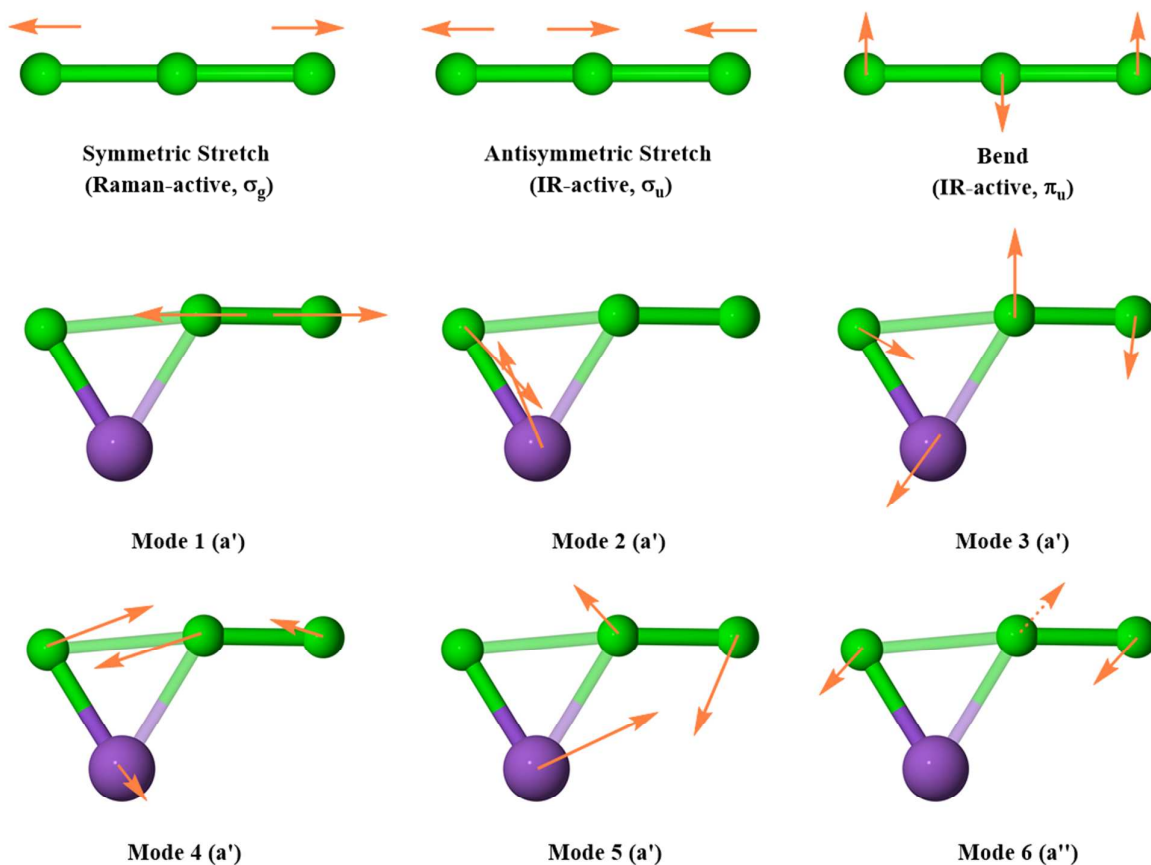


Figure 5. Vibrational modes for the D_{oh} “free” X_3^- (illustrated for Cl_3^-) and C_s MX_3 (illustrated for KCl_3).

In Table 3, the harmonic vibrational frequencies of the isolated X_3^- computed in this work agree to within 3 cm^{-1} of those reported by Dixon and coworkers.⁵ However, with respect to the experimental MCl_3 frequencies (see Table 4) of Ault and Andrews,³ we only observed reasonable agreement with the 258 cm^{-1} band for KCl_3 . In fact, the experimental frequencies of the two prospective MCl_3 bands range from $327 - 410\text{ cm}^{-1}$ and $225 - 276\text{ cm}^{-1}$, respectively.³ A similar range is also noticed for our computed MCl_3 frequencies. It is unclear why the two stretch frequencies of Cl_3^- vary so greatly over the range of alkali metal counterions. The extended ranges for the computed MBr_3 and MI_3 frequencies (Table 5-6) imply a similar ambiguity. This calls into question

whether the two observed MX_3 bands truly correspond to the symmetric and antisymmetric stretches of X_3^- . Rather, the bonding in MX_3 establishes alternate normal modes of vibration that include substantial displacement of both the halide and metal. Therefore, a direct comparison of the frequencies of X_3^- and MX_3 is not straightforward, and explicit inclusion of the alkali metal cation is necessary.

TABLE 3. Harmonic vibrational frequencies (cm^{-1}) and infrared intensities (in parentheses, km mol^{-1}) for the isolated X_3^- ($\text{X} = \text{Cl}, \text{Br}, \text{and I}$) anions computed using the CCSD(T)/AWCVTZ method.

Mode	Cl_3^-		Br_3^-		I_3^-	
	ω^a	ω^b	ω^a	ω^b	ω^a	ω^b
ω_1 (asym stretch, σ_u)	253 (623) ^c	254	187 (250)	186	138 (151)	139
ω_2 (sym stretch, σ_g)	264 (0) ^c	261	164 (0)	161	114 (0)	112
ω_3 (bend, π_u)	161 (1)	159	89 (0)	88	57 (0)	57

^a Harmonic vibrational frequencies in this work. ^b Harmonic vibrational frequencies reported by Dixon and coworkers (ref. 5). ^c Vibrational modes for ω_1 and ω_2 switch for Cl_3^- .

TABLE 4. Harmonic vibrational frequencies (cm^{-1}) and infrared intensities (in parentheses, km mol^{-1}) of the chlorides MCl_3 ($\text{M} = \text{Li}, \text{Na}, \text{K}, \text{Rb}, \text{and Cs}$) molecules predicted using the CCSD(T)/AWCVTZ method.

	LiCl_3		NaCl_3		KCl_3		RbCl_3		CsCl_3	
	ω	<i>expt</i> ^a	ω	<i>expt</i> ^a	ω	<i>expt</i> ^a	ω	<i>expt</i> ^a	ω	<i>expt</i> ^a
ν_1 (a') ^b	453 (93)	410	414 (188)	375	370 (242)	345	360 (245)	340	354 (239)	327
ν_2 (a') ^b	576 (107)	-	322 (41)	276	248 (57)	258	222 (80)	223	216 (89)	225
ν_3 (a') ^b	281 (84)		183 (25)		190 (16)		179 (10)		174 (27)	
ν_4 (a') ^b	92 (77)		117 (113)		138 (158)		134 (140)		127 (116)	
ν_5 (a') ^b	124 (5)		85 (8)		66 (2)		52 (1)		44 (1)	
ν_6 (a'') ^b	108 (7)		123 (1)		138 (1)		141 (1)		143 (1)	

^a Raman and IR fundamentals reported in the Ault and Andrews argon matrix study (ref. 3). ^b The ν_{1-6} correspond to the modes 1-6 in Figure 5, respectively.

A Complex of MX with X₂?

The idea that the alkali metal trihalides might be viewed (that's all, just a suggestion of an alternative perspective) as strongly bound complexes of MX and X₂ came from examining the detailed nature of the fundamental vibrations of these molecules.

As depicted in Figure 5, the antisymmetric and symmetric stretches of X₃⁻ proposed in the previous experimental study³ of MX₃ are not found among our computed vibrational modes of MX₃. Note that the modes illustrated in Figure 5 are similar in all MX₃ (M = Li, Na, K, Rb, Cs and X = Cl, Br, I) molecules. However, for the species with heavy metals (Rb and Cs) which show relatively mild perturbation to X₃⁻ (judging from its distance asymmetry in Table 2), mode 2 (M-X1 stretch) is coupled with the adjacent X1-X2 stretch. Still, no sign of any well-preserved symmetric or antisymmetric stretches of the “free” X₃⁻ anion can be found from the modes of MX₃.

Figure 5 illustrates the vibrational modes for KCl₃. The fundamental vibrations of other MX₃ molecules are remarkably similar, despite the difference in internal asymmetry of the X₃ unit, and distance of M from X₃. There are differences, which may be seen by comparing KCl₃ and MX₃, illustrated in SI. We also found useful a Total Energy Distribution (TED) analysis of the vibrations, which allows one to see the internal coordinates entering a given vibration. These are tabulated in the SI (Table S1). A file allowing animation of all vibrations is available from the authors.

Only modes 1 and 6 involve displacement of the halides alone, whereas modes 2, 3, 4, and 5 involve significant displacements of the metal as well. Note that mode 1 is almost a pure X-X bond stretch; however, the stretch appears localized to a single X-X bond (X2-X3, B2 in Figure 3), unlike the stretches of X₃⁻ which displace two X-X bonds. This is not unexpected; the equilibrium geometries of the X₃⁻ unit in MX₃ are unsymmetrical in just this direction. Mode 2 appears to be a

1
2
3 localized M-X (M and X1, B3 in Figure 3) bond stretch. This localization of two fundamental modes
4
5 of vibration, conserved across the series studied, suggests that the MX_3 system may be alternatively
6
7 described as an MX-X_2 complex, rather than a M^+X_3^- ion pair. On this basis, modes 1 and 2 should
8
9 be distorted X-X and M-X stretches. Specifically, compared to the “free” X_2 and MX frequencies
10
11 (Table 1), the localized X-X and M-X stretch frequencies of the MX_3 species (Tables 4-6) are mostly
12
13 found to be lowered, and a consistently decreasing trend may be found moving from Li to Cs.
14
15
16

17
18 We note in passing that the optimized bond distances also show a sign of $\text{MX}\square\square\square\text{X}_2$ bonding –
19
20 the X1-X2 distance is always longer than X2-X3, and M-X1 is shorter than M-X2. Agreed, the
21
22 differences are not large, but the trend is consistent.
23
24

25
26 While we question the previous description of the MX_3 normal modes, the corresponding
27
28 frequencies computed here should still align with the experimental vibrational bands. This is because
29
30 all the modes belong to irreducible representations of the C_s point group, and are thus both
31
32 IR/Raman-active. So a detailed comparison with matrix isolation experiment is in order.
33
34

35
36 As shown in Tables 3 and 4, a direct comparison of the MCl_3 harmonic vibrational frequencies
37
38 with the experimental values of Ault and Andrews³ yields generally better agreement than the
39
40 previous comparison using Cl_3^- , isolated, noninteracting vibrational modes. To facilitate the
41
42 assignment of the experimental bands, we notice that only a few modes have the intensity necessary
43
44 for detection. In addition, the noted IR spectrophotometer limit (200 cm^{-1}) of the experiment³
45
46 precludes the observation of $\nu_4 - \nu_6$ for LiCl_3 and $\nu_3 - \nu_6$ for MCl_3 (M = Na, K, Rb, and Cs).
47
48 Therefore, only ν_1 and ν_2 are candidates for assignment to the experimental IR/Raman bands.
49
50
51

52
53 The harmonic vibrational frequencies corresponding to ν_1 and ν_2 of the MCl_3 molecules are
54
55 relatively close to the experimental values. However, there remain significant discrepancies.
56
57

1
2
3
4 Deviations above 40 cm^{-1} from fundamentals are noticed for ν_1 and ν_2 of LiCl_3 and NaCl_3 . The ν_2
5
6 harmonic vibrational frequencies for KCl_3 , RbCl_3 , and CsCl_3 deviate by $20\text{--}27\text{ cm}^{-1}$, which is more
7
8 reasonable, but still larger than expected. For the frequencies of this magnitude, we do not expect
9
10 substantially large enough anharmonic contributions to correct these deviations. A plausible reason
11
12 for such deviations is that the large red-shift (about $20 - 60\text{ cm}^{-1}$, see Table S1 in the SI) noted for
13
14 MX vibrational fundamentals in argon matrices⁸ carries over to the MX_3 species. Recall that in Ault
15
16 and Andrews's experiment,³ MCl_3 was generated through the reaction of MCl and Cl_2 in an argon
17
18 matrix at 15 K. As such, the MCl stretch was measured prior to MCl_3 formation. This stretch
19
20 frequency aligns with the value reported by Jacox (see Table S1 in the SI),^{8,79} confirming a similar
21
22 argon-induced shift for the Ault and Andrews MCl band. By extension, their reported MCl_3 bands
23
24 may be significantly shifted as well. Accordingly, assessing the agreement between gas-phase
25
26 theoretical frequencies and argon matrix experimental frequencies³ is challenging. Depending on the
27
28 metal involved, ν_1 and ν_2 can be tentatively assigned to the Cl-Cl and M-Cl stretches, which are
29
30 probably the actual vibrational bands observed in the Ault and Andrews experiment.³
31
32
33
34
35
36
37

38 In comparison, there are fewer experimental results for the MBr_3 (Table 5) and MI_3 (Table 6)
39
40 species. The 214 cm^{-1} KBr_3 band reported by Ault and Andrews³ is close to our computed frequency
41
42 for the localized Br-Br stretch mode ($\nu_1 = 225\text{ cm}^{-1}$). Since the largest vibrational frequency of the
43
44 “free” Br_3^- is predicted to be 187 cm^{-1} (Table 3), it is not reasonable to assign this 214 cm^{-1} band to
45
46 Br_3^- in KBr_3 . A good agreement between theory and experiments^{6,7,16,80} is achieved for the CsBr_3
47
48 vibrational frequencies. The ν_1 , ν_2 , and ν_4 frequencies are computed to be 217, 152, and 96 cm^{-1} ,
49
50 respectively, each of which matches the observed vibrational bands within 10 cm^{-1} . Comparison of
51
52 the computed frequencies of CsBr_3 (Table 5) and the “free” Br_3^- (Table 3) indicate that the 152 and
53
54
55
56
57
58
59
60

96 cm^{-1} experimental bands seemingly match those of Br_3^- , whereas the 217 cm^{-1} band does not.

TABLE 5. Harmonic vibrational frequencies (cm^{-1}) and infrared intensities (in parentheses, km mol^{-1}) of the bromides MBr_3 ($\text{M} = \text{Li, Na, K, Rb, and Cs}$) molecules predicted using the CCSD(T)/AWCVTZ method. The KBr_3 and CsBr_3 frequencies in italics are from experiments.

	LiBr_3	NaBr_3	KBr_3	RbBr_3	CsBr_3
$\nu_1 (a)^\text{a}$	244 (72)	227 (81)	225 (134), <i>214^b</i>	220 (137)	217 (138), <i>206^c/210^d/213^e</i>
$\nu_2 (a)^\text{a}$	475 (88)	258 (67)	183 (23)	155 (32)	152 (40), <i>140^e/136^d/138^e</i>
$\nu_3 (a)^\text{a}$	283 (79)	150 (26)	141 (38)	128 (14)	122 (4)
$\nu_4 (a)^\text{a}$	104 (38)	108 (47)	113 (31)	106 (30)	96 (27), <i>82^e</i>
$\nu_5 (a)^\text{a}$	76 (17)	66 (6)	50 (3)	37 (2)	29 (1)
$\nu_6 (a)^\text{a}$	77 (6)	79 (1)	82 (0)	83 (0)	84 (0)

^a The ν_{1-6} correspond to the modes 1-6 in Figure 5, respectively. ^b Raman and IR frequencies reported in ref. 3. ^c Raman and IR frequencies reported in refs. 6 and 7. ^d IR frequencies reported in ref. 80. ^e Raman frequencies reported in ref. 16.

TABLE 6. Harmonic vibrational frequencies (cm^{-1}) and infrared intensities (in parentheses, km mol^{-1}) of the iodides MI_3 ($\text{M} = \text{Li, Na, K, Rb, and Cs}$) molecules predicted using the CCSD(T)/AWCVTZ method. The CsI_3 frequencies in italics are from experiments.

	LiI_3	NaI_3	KI_3	RbI_3	CsI_3
$\nu_1 (a)^\text{a}$	171 (56)	164 (69)	168 (67)	160 (87)	157 (88), <i>145^b/145^c/149^d</i>
$\nu_2 (a)^\text{a}$	417 (79)	222 (37)	149 (40)	118 (12)	110 (17), <i>101^b/100^c/103^d/113^e</i>
$\nu_3 (a)^\text{a}$	273 (58)	130 (16)	106 (23)	96 (22)	90 (11)
$\nu_4 (a)^\text{a}$	80 (26)	83 (27)	86 (16)	79 (10)	74 (12), <i>66^c/69^d</i>
$\nu_5 (a)^\text{a}$	51 (7)	47 (4)	39 (4)	30 (2)	24 (1)
$\nu_6 (a)^\text{a}$	53 (8)	51 (1)	53 (0)	53 (0)	54 (0)

^a The ν_{1-6} correspond to the modes 1-6 in Figure 5, respectively. ^b Raman and IR frequencies reported in refs. 6 and 7. ^c IR frequencies reported in ref. 80. ^d IR frequencies reported in ref. 81. ^e Raman fundamental (in solid argon) reported in ref. 4.

1
2
3
4 For CsI_3 , we find that the three vibrational frequencies from experiments^{6, 7, 80, 81} align well with
5
6 our predicted harmonic values for ν_1 , ν_2 , and ν_4 . It should be noted that each of the three computed
7
8 frequencies of “free” I_3^- (Table 3) are in relatively good agreement with the corresponding
9
10 experimental values for ν_1 , ν_2 , and ν_4 of CsI_3 (Table 6). This is the only case where X_3^- completely
11
12 corresponds with MX_3 . However, CsI_3 is an extreme case, for which the frequencies (and the
13
14 geometry) tend to suggest a Cs^+I_3^- ion pair, in spite of its underlying electronic structure (see next
15
16 section). More generally, the experimental frequencies of CsBr_3 and CsI_3 were obtained from the
17
18 solid state,^{6, 7, 16, 80, 81} which might involve alternate electronic structures that make a direct
19
20 comparison between theory and experiment ambiguous. The seemingly aligned I_3^- and CsI_3
21
22 frequencies are outliers. They by no means guarantee overall agreement across all MBr_3 and MI_3 (M
23
24 = Li, Na, K, Rb, and Cs) species.
25
26
27
28
29

30 To summarize: with limited experimental data, no solid conclusion can be drawn here from the
31
32 experimentally observed vibrations about whether the MBr_3 and MI_3 should be viewed more as an
33
34 M^+X_3^- ion pair or the MX-X_2 complex. These concerns notwithstanding, explicit consideration of the
35
36 metal is instrumental in understanding the vibrational frequencies of the MX_3 species. And an
37
38 MX-X_2 complex viewpoint of the bonding in the molecule, a perspective that has hitherto not
39
40 received much attention, is naturally suggested by the vibrational modes. Key factors driving the
41
42 vibrational frequencies are clearly evinced by an intimate examination of the electronic structure
43
44 through bonding analyses.
45
46
47
48
49
50
51
52
53
54
55
56
57
58
59
60

Bonding Analyses of MX_3

Bond strength has been described theoretically in the literature by a plethora of bonding indices. Just the fact that there are so many is evidence that bond indices, even as they carefully defined, are to some degree arbitrary. We chose to follow here the insight obtained from a natural bond orbital bond order, as defined by Weinhold and Landis.⁸² The natural bond orbital (NBO) results in Table 7 show that the bond order of B1 (X1-X2) is consistently lower than that of B2 (X2-X3) for each MX_3 species. No surprise, as this follows the calculated equilibrium distances. A considerable increase of X1-X2 bond order indicates the X1-X2 and X2-X3 become more balanced for KBr_3 , RbBr_3 , CsBr_3 , KI_3 , RbI_3 , and CsI_3 . For the MCl_3 species, the X2-X3 bond orders are large, approaching those of a single bond. But as the distances in Table 2 show, the corresponding bond length remains substantially longer than in Cl_2 .

In the NBO formalism, it is possible to assign covalent and ionic character to bonds.⁵⁹⁻⁶¹ The covalency of the X2-X3 bond is also supported by its natural bond order, comprised primarily of covalent contributions (Table 7), although an increasing ionic character of the X2-X3 bond can be found on moving from LiCl_3 to CsCl_3 . The preference of covalent over ionic character is switched for KBr_3 , RbBr_3 , CsBr_3 , KI_3 , RbI_3 , and CsI_3 , in which the X2-X3 bonds possess slightly more ionic features than covalency. This is in accordance with the increased negative charges on atom X3, as shown in Table 7.

The calculated charge distribution shows almost complete electron transfer from the metal ion to the trihalide. And in the trihalide, no matter how asymmetric it is, the net charge on the central atom, X1 is close to zero. The electron transferred is distributed, in an asymmetric fashion consistent with the asymmetry of the bonding, among X1 and X3. The pileup of electron density at the termini of a

1
2
3 three-center electron-rich system is what one would expect; it is connected, in another context, to the
4 presence of strongly electronegative fluorides at the termini and not the middle of such bonds (e.g.
5
6
7
8
9
10
11
12
13
14
15
16
17
18
19
20
21
22
23
24
25
26
27
28
29
30
31
32
33
34
35
36
37
38
39
40
41
42
43
44
45
46
47
48
49
50
51
52
53
54
55
56
57
58
59
60
FXeF).

The presence of the metal cation engenders localization of electron density mostly onto X1, as shown by the natural charges in Table 7. Orbital interactions based on the NBO perturbation theory analysis (see Methods) shows that the leading interaction between the X1 and X2-X3 units is always the donation of an X1 lone-pair $n(X1)$ into the X2-X3 antibonding orbital $\sigma^*(X2-X3)$ for all MX_3 species. Thus, strengthened X1-X2 and weakened X2-X3 bonds are expected. The energies for this $n(X1) \rightarrow \sigma^*(X2-X3)$ interaction (see SI) gradually increase from LiX_3 to CsX_3 (X = Cl, Br, or I). Therefore, the bond orders of X1-X2 and X2-X3 are expected to increase and decrease, respectively. This finding aligns with the trends for the natural bond orders of X1-X2 and X2-X3 given in Table 7. Also, this is in consistent with the decreasing X1-X2 and increasing X2-X3 bond lengths in Table 2.

The general picture that emerges is consistent with the donor-acceptor picture of bonding in the trihalide anions, at one end of a bonding spectrum, at the other end being symmetrical electron-rich bonding.²⁰⁻²⁴

TABLE 7. Natural bond orders and natural charges for MX_3 .^a

	Natural bond order: total (covalent/ionic)				Natural charge			
	X1-X2 (B1)	X2-X3 (B2)	X1-M (B3)	X2-M (B4)	X1	X2	X3	M
Cl_3^-	0.50 (0.25/0.25)	0.50 (0.25/0.25)	-	-	-0.48	-0.03	-0.48	-
LiCl_3	0.06 (0.00/0.06)	0.90 (0.82/0.08)	0.50 (0.02/0.48)	0.43 (0.01/0.42)	-0.88	0.00	-0.05	0.93
NaCl_3	0.08 (0.01/0.07)	0.86 (0.73/0.13)	0.89 (0.02/0.87)	0.01 (0.00/0.01)	-0.86	0.01	-0.11	0.96
KCl_3	0.13 (0.03/0.10)	0.79 (0.61/0.18)	0.75 (0.01/0.74)	0.06 (0.00/0.06)	-0.81	0.01	-0.18	0.97
RbCl_3	0.15 (0.04/0.11)	0.77 (0.57/0.20)	0.72 (0.01/0.71)	0.06 (0.00/0.06)	-0.79	0.01	-0.20	0.98
CsCl_3	0.16 (0.04/0.12)	0.75 (0.54/0.21)	0.69 (0.01/0.68)	0.07 (0.00/0.07)	-0.79	0.01	-0.21	0.98
Br_3^-	0.50 (0.25/0.25)	0.50 (0.25/0.25)	-	-	-0.48	-0.03	-0.48	-
LiBr_3	0.13 (0.03/0.10)	0.76 (0.62/0.14)	0.47 (0.02/0.45)	0.43 (0.01/0.42)	-0.77	-0.01	-0.14	0.92
NaBr_3	0.15 (0.04/0.11)	0.75 (0.56/0.19)	0.74 (0.02/0.72)	0.06 (0.00/0.09)	-0.76	0.00	-0.20	0.96
KBr_3	0.30 (0.11/0.18)	0.56 (0.25/0.31)	0.25 (0.00/0.25)	0.19 (0.00/0.19)	-0.71	0.00	-0.26	0.97
RbBr_3	0.31 (0.12/0.19)	0.55 (0.24/0.31)	0.23 (0.00/0.23)	0.20 (0.00/0.20)	-0.70	0.01	-0.28	0.97
CsBr_3	0.32 (0.13/0.19)	0.54 (0.23/0.31)	0.23 (0.00/0.23)	0.20 (0.00/0.20)	-0.68	0.01	-0.30	0.98
I_3^-	0.50 (0.25/0.25)	0.50 (0.25/0.25)	-	-	-0.49	-0.03	-0.49	-
LiI_3	0.15 (0.03/0.12)	0.77 (0.60/0.17)	0.53 (0.03/0.50)	0.32 (0.01/0.31)	-0.73	-0.01	-0.16	0.89
NaI_3	0.17 (0.05/0.12)	0.74 (0.54/0.20)	0.58 (0.02/0.56)	0.26 (0.00/0.26)	-0.72	-0.01	-0.21	0.94
KI_3	0.31 (0.12/0.19)	0.55 (0.25/0.30)	0.44 (0.01/0.43)	0.10 (0.00/0.10)	-0.69	0.00	-0.27	0.96
RbI_3	0.32 (0.13/0.19)	0.54 (0.24/0.30)	0.24 (0.00/0.24)	0.21 (0.00/0.24)	-0.68	0.00	-0.29	0.97
CsI_3	0.33 (0.14/0.19)	0.53 (0.23/0.30)	0.24 (0.00/0.24)	0.21 (0.00/0.21)	-0.67	0.00	-0.31	0.97

^a The CCSD(T)/AWCVTZ geometries are used. See Figure 2 for atomic label and bond definition for MX_3 .

Both B3 (X1-M) and B4 (X2-M) bonds possess some “purely” ionic character, supported by the natural charges and their predominant ionic bond orders reported in Table 7. For the MCl_3 series, except for the similar X1-M and X2-M bond orders for LiCl_3 , the X1-M bond orders for the other species are much higher than the X2-M bond orders, but comparable to the corresponding X2-X3 (B2) covalent bonds. This observation supports a view of MCl_3 as formed from MX and X_2 interacting through weaker X1-X2 and X2-M bonds. For the bromides and iodides, however, a considerably decreased X1-M bond order for KBr_3 , RbBr_3 , CsBr_3 , KI_3 , RbI_3 , and CsI_3 can be noticed,

1
2
3
4 coupled to the generally increased X1-X2 and X2-M bond orders. This is another indication that the
5
6 X_3^- is less impacted by the larger metal atoms than the smaller ones, which also leaves these species
7
8 standing at a borderline between the MX-X₂ complex and M⁺X₃⁻ ion pair. However, the featured
9
10 antisymmetric and symmetric stretches of X₃⁻ are not clearly exhibited in their vibrational modes
11
12 discussed previously.
13
14

15
16 To further correlate the NBO results with the vibrational frequencies, the gradually increasing
17
18 interaction energies (see SI) for the donor-acceptor interaction [$n(X1) \rightarrow \sigma^*(X2-X3)$] from LiX₃ to
19
20 CsX₃ rationalize the increasingly shifted X-X stretch frequencies (Tables 4-6) in MX₃, relative to the
21
22 frequencies of corresponding “free” diatomic X₂ species (Table 1). The increasing dative interaction
23
24 from Li to Cs leads to a greater $\sigma^*(X2-X3)$ orbital occupation, which weakens the X2-X3 bond (B2)
25
26 and therefore lowers the X-X stretch frequencies. On the other hand, a comparison of the M-X
27
28 stretch frequencies of MX₃ and the “free” MX shows that the X1-M (B3) stretch in MX₃ becomes
29
30 decreasingly impacted from Li to Cs. The physical origins of this trend seem ambiguous. One
31
32 possible explanation is that its displacement of the metal in the M-X1 stretch decreases as it becomes
33
34 heavier, making any perturbation from the X₂ moiety have less impact.
35
36
37
38
39
40
41
42
43
44
45
46
47
48
49
50
51
52
53
54
55
56
57
58
59
60

QTAIM

All of the molecules studied feature bond critical points for every short contact. This is shown in Fig. 6 for a typical molecule, KCl_3 .

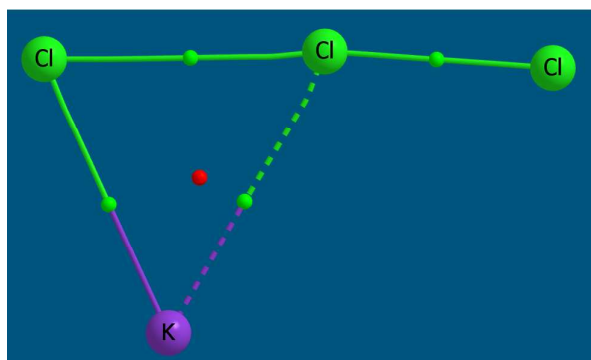


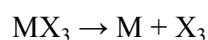
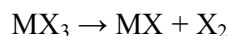
Figure 6. Bader analysis for the C_s MX_3 (illustrated for KCl_3), including bond critical points (BCPs, green) and ring critical point (RCP, red). The dashed line for the central KCl bond indicates a CP density below the “weak CP threshold” of 0.025 a.u.

Our results from Bader’s quantum theory of atoms-in-molecules (QTAIM) are reported in detail in the SI. Consistent with above NBO results (Table 7), the electron density at the bond critical points (BCPs) of B1 (X1-X2) is lower than that of B2 (X2-X3) for each MX_3 species, suggesting a consistently stronger X2-X3 bond than the X1-X2 bond. Similar to the NBO results from LiX_3 to CsX_3 , the trends in BCP densities of the X1-X2 bonds (increasing) and X2-X3 bonds (decreasing) indicate that the two bonds become more balanced. In Bader’s characterization of atomic interactions,⁸³ the Laplacian of the electron densities $\nabla^2\rho(\text{BCP})$ in Table S2 (in the SI) should provide general bonding features of the MX_3 systems. The consistently smaller $\nabla^2\rho(\text{BCP})$ of the bond X2-X3 compared to that of the X1-X2 bond implies that the former possesses more covalency than the later. In addition, the X2-X3 $\nabla^2\rho(\text{BCP})$ increases from LiX_3 to CsX_3 , suggesting an increasing ionic and decreasing covalent character.

1
2
3
4 In summary, the bonding trends explored with NBO and QTAIM approaches clearly show that
5
6 X1-X2 and X2-X3 become more balanced from LiX_3 to CsX_3 , although they are never as “truly”
7
8 balanced as in the “free” D_{oh} symmetric X_3^- . We are led to the same conclusion drawn from the
9
10 structures (Table 2) of MX_3 : a decreasing effect of the M^+ cation on the X_3^- anions from LiX_3 to
11
12 CsX_3 . A comparison of the bonding types of X_3^- (Scheme 1) and MX_3 (Table 7) shows that the two
13
14 equal contributors (bonding types I and II) to the bonding in X_3^- anions collapse into mostly just one
15
16 of the two for MX_3 , mainly depending on the position of the metal cations.
17
18
19
20
21
22
23
24

25 Thermochemistry of MX_3

26
27 The reaction energies (D_0 , corrected by ZPVE) of three different dissociation pathways:



31
32
33
34
35
36
37 are summarized in Table 8. The reason for studying the neutral version of the $\text{MX}_3 \rightarrow \text{M}^+ + \text{X}_3^-$
38
39 fragmentation is that ionic fragmentation is naturally more endothermic than neutral ones. In all
40
41 cases, the dissociation energy for the $\text{MX}_3 \rightarrow \text{MX} + \text{X}_2$ reaction is much lower than that of the MX_3
42
43 $\rightarrow \text{M}^+ + \text{X}_3^-$ (or $\text{MX}_3 \rightarrow \text{M} + \text{X}_3$) dissociation. This result supports our previous conclusion
44
45 indicating that the MX_3 system is also well-described as an MX-X_2 complex, rather than an M^+X_3^-
46
47
48
49
50 ion pair.
51
52
53
54
55
56
57
58
59
60

TABLE 8. Endothermicities (D_0 , kcal mol⁻¹) of the three different dissociation processes for MX_3 (M = Li, Na, K, Rb, and Cs; X = Cl, Br, and I) molecules predicted using the B3LYP3/AVTZ method.

Species	D_0 ($\text{MX}_3 \rightarrow \text{MX} + \text{X}_2$)	D_0 ($\text{MX}_3 \rightarrow \text{M}^+ + \text{X}_3^-$)	D_0 ($\text{MX}_3 \rightarrow \text{M} + \text{X}_3$)
LiCl ₃	10.0	134.8	115.1
NaCl ₃	11.2	114.1	99.0
KCl ₃	12.9	100.3	105.6
RbCl ₃	13.3	95.8	105.8
CsCl ₃	13.1	91.6	108.9
LiBr ₃	14.3	127.6	101.8
NaBr ₃	15.3	109.1	87.9
KBr ₃	17.5	95.7	95.0
RbBr ₃	17.9	91.3	95.3
CsBr ₃	18.0	87.3	98.6
LiI ₃	15.0	120.7	88.4
NaI ₃	15.2	104.0	76.3
KI ₃	17.3	90.5	83.2
RbI ₃	17.5	86.0	83.4
CsI ₃	18.1	82.2	87.0

A note on the numbers in the last two columns: the energetics is a reflection of the differences in the ionization potentials of the metal atoms (falling from 5.5 eV for Li to 3.9 eV for Cs), and the vertical electron affinities of the neutral X_3 species. The latter are remarkably high, 4-5 eV. For the $\text{MX}_3 \rightarrow \text{MX} + \text{X}_2$ dissociation, an increasing trend for D_0 can be noticed from LiX_3 to CsX_3 (X = Cl, Br, or I). This is consistent with the increasing trend for D_0 in the fluoride $\text{MF}_3 \rightarrow \text{MF} + \text{F}_2$ (M = Na, K, Rb, and Cs) series reported by Tozer and Sosa²⁹. In addition, previous experiments determined the bond strengths ($\text{X}_3^- \rightarrow \text{X}_2 + \text{X}^-$) of the isolated Cl_3^- , Br_3^- , and I_3^- to be about 24, 30, and 30 kcal mol⁻¹ in the gas phase, respectively.^{9, 10} Those values are about the twice the D_0 values computed here for the $\text{MX}_3 \rightarrow \text{MX} + \text{X}_2$ dissociations. This is additional evidence that presence of an alkali metal cation weakens the X-X covalent band of X_3^- , favoring localization of more electron density on a terminal X atom. For the $\text{MX}_3 \rightarrow \text{M}^+ + \text{X}_3^-$ dissociation, a decreasing trend in D_0 can be found

1
2
3 from LiX_3 to CsX_3 ($X = \text{Cl}, \text{Br}, \text{or I}$). This indicates that the distortion of X_3^- by M^+ decreases with
4
5 increasing cation size, caused by the increasing distance between M^+ and X^- as well as the
6
7 decreasing M-X orbital overlap from LiX_3 to CsX_3 . This agrees well with the structural trend for
8
9 increasingly balanced X1-X2 and X2-X3 bond lengths (Figure 3 and Table 2) moving from LiX_3 to
10
11
12
13 CsX_3 .

18 **Conclusions**

19
20 The alkali metal trihalides MX_3 ($\text{M} = \text{Li}, \text{Na}, \text{K}, \text{Rb}, \text{Cs}$; and $\text{X} = \text{Cl}, \text{Br}, \text{I}$) are systematically
21
22 studied here using coupled-cluster methods with the weighted core-valence correlation consistent
23
24 basis sets (new basis sets for K, Rb, and Cs). Benchmarks comparing the CCSD(T) method against
25
26 experimental results show satisfactory performance for the new basis sets in predicting reliable
27
28 structures and harmonic vibrational frequencies for the relevant diatomic species MX and X_2 . An
29
30 isomer search using the B3LYP functional confirms a planar asymmetric T-shaped structure as the
31
32
33 global minimum for all MX_3 species.

34
35 The CCSD(T) computations suggest a strong distortion of the X_3^- anions by the alkali metal
36
37 counterocations M^+ , in the equilibrium geometries, vibrational spectra, bonding, and thermochemistry.
38
39 For the vibrational modes, the well-established antisymmetric and symmetric stretches of the “free”
40
41 X_3^- anions are not retained in any MX_3 species. Instead, localized and mutually-perturbed X-X and
42
43 M-X stretches are involved. For the vibrational frequencies, a comparison of our theoretical MX_3
44
45 harmonic vibrational frequencies with the experimental fundamentals yields generally better
46
47 agreement than the previous comparison using the “free” X_3^- anions. In a bonding analysis, the NBO
48
49 and QTAIM results show low natural bond orders and electron densities at the bond critical points
50
51
52
53
54
55
56

1
2
3 between MX and X₂, respectively. In the thermochemistry, the MX₃ → MX + X₂ dissociation
4
5 pathway has a much smaller endothermicity than the MX₃ → M⁺ + X₃⁻ (or MX₃ → M + X₃) pathway.
6
7 All above results lead us to suggest that the MX₃ system might alternatively be described as an
8
9 MX-X₂ complex, rather than the M⁺X₃⁻ ion pair proposed in previous studies.¹⁻⁴
10
11

12
13 Our conclusions are likely applicable only to the MX₃ systems in the gas phase, in inert matrices
14
15 (argon and neon), or in non-polar solvents if possible, as no strong solvation would be expected.
16
17 Strong solvation of M⁺ and X₃⁻ ions in polar solvents (H₂O, for instance) could make the M⁺X₃⁻ ion
18
19 pair an appropriate description for the MX₃ systems. Such solvation phenomena on the molecular
20
21 and electronic structure of X₃⁻ are known as a crucial part of understanding their electrochemistry in
22
23 electrolytic media,^{84, 85} a subject beyond present study.
24
25
26

27
28 The two perspectives on MX₃ molecules – strong complexation of trihalide anions by metal
29
30 cations, and strong interaction of polar MX molecules with dihalogens -- are complementary to each
31
32 other, each with its own advantages and consequences. We think the chemistry of these remarkable
33
34 molecules will benefit from keeping both pictures of the bonding in them in view.
35
36
37
38
39
40
41
42

43 **Supporting Information**

44
45 The Supporting Information is available free of charge on the ACS Publications website.

46
47 Convergence parameters used for programs, the cc-pwCVTZ-PP basis sets for K, Rb, and Cs, and
48
49 the detailed information of all species.
50
51
52
53
54
55
56
57
58
59
60

Acknowledgments

This research was supported by the U.S. National Science Foundation (Grant No. CHE-1361178) and the Engineering and Physical Sciences Research Council (UK, project EP/N02253X/1). We thank Professor Frank A. Weinhold (University of Wisconsin–Madison) and Dr. Yaoming Xie (CCQC, University of Georgia) for helpful discussions concerning the NBO analyses.

References

- (1) Ault, B. S.; Andrews, L. Salt-Molecule Matrix Reactions. Infrared Spectra of the $M^+HCl_2^-$ and $M^+Cl_3^-$ Ion Pairs in Solid Argon. *J. Am. Chem. Soc.* **1975**, *97*, 3824-3826.
- (2) Andrews, L. Optical Spectra of the Difluoride, Dichloride, and Trichloride Ions in the Matrix-Isolated $M^+F_2^-$, $M^+Cl_2^-$, and $M^+Cl_3^-$ Species. *J. Am. Chem. Soc.* **1976**, *98*, 2147-2152.
- (3) Ault, B. S.; Andrews, L. Infrared and Raman Spectra of the $M^+Cl_3^-$ Ion Pairs and Their Chlorine–Bromine Counterparts Isolated in Argon Matrices. *J. Chem. Phys.* **1976**, *64*, 4853-4859.
- (4) Andrews, L.; Prochaska, E. S.; Loewenschuss, A. Resonance Raman and Ultraviolet Absorption Spectra of the Triiodide Ion Produced by Alkali Iodide-Iodine Argon Matrix Reactions. *Inorg. Chem.* **1980**, *19*, 463-465.
- (5) Thanthiriwatte, K. S.; Spruell, J. M.; Dixon, D. A.; Christe, K. O.; Jenkins, H. D. B. Structures, Vibrational Frequencies, and Stabilities of Halogen Cluster Anions and Cations, $X_n^{+/-}$, $n = 3, 4$, and 5 . *Inorg. Chem.* **2014**, *53*, 8136-8146.
- (6) Gabes, W.; Gerding, H. Vibrational Spectra and Structures of the Trihalide Ions. *J. Mol. Struct.* **1972**, *14*, 267-279.
- (7) Gabes, W.; Elst, R. Force Constants of the Trihalide Ions. *J. Mol. Struct.* **1974**, *21*, 1-5.
- (8) Jacox, M. E. Comparison of the Ground State Vibrational Fundamentals of Diatomic Molecules in the Gas Phase and in Inert Solid Matrices. *J. Mol. Spectrosc.* **1985**, *113*, 286-301.
- (9) Do, K.; Klein, T. P.; Pommerening, C. A.; Sunderlin, L. S. A New Flowing Afterglow-Guided Ion Beam Tandem Mass Spectrometer. Applications to the Thermochemistry of Polyiodide Ions. *J. Am. Soc. Mass. Spectrom.* **1997**, *8*, 688-696.

- 1
2
3 (10) Nizzi, K. E.; Pommerening, C. A.; Sunderlin, L. S. Gas-Phase Thermochemistry of Polyhalide Anions. *J.*
4 *Phys. Chem. A* **1998**, *102*, 7674-7679.
5
6
7 (11) Person, W. B.; Anderson, G. R.; Fordemwalt, J. N.; Stammreich, H.; Forneris, R. Infrared and Raman
8 Spectra, Force Constants, and the Structures of Some Polyhalide Ions: ICl_2^- , ICl_4^- , BrCl_2^- , and Br_3^- . *J. Chem.*
9 *Phys.* **1961**, *35*, 908-914.
10
11
12 (12) Nelson, I. V.; Iwamoto, R. T. Voltammetric Evaluation of the Stability of Trichloride, Tribromide, and
13 Triiodide Ions in Nitromethane, Acetone, and Acetonitrile. *J. Electroanal. Chem. (1959)* **1964**, *7*, 218-221.
14
15
16 (13) Robertson, K. N.; Cameron, T. S.; Knop, O. Polyhalide Anions in Crystals. Part 2. I_3^- Asymmetry and
17 $\text{NH}\cdots\text{I}$ Bonding: Triiodides of the Me_2NH_2^+ , Ph_2I^+ , Tropanium, *N,N,N',N'*-Me₄-1,2-ethanediammonium,
18 *N,N,N',N'*-Me₄-1,3-propanediammonium, *N*-Me-piperazinium(2+), and *N,N'*-Me₂-piperazinium(2+) Cations,
19 and $\text{Me}_2\text{NH}_2\text{I}$. *Can. J. Chem.* **1996**, *74*, 1572-1591.
20
21
22
23 (14) Robertson, K. N.; Bakshi, P. K.; Cameron, T. S.; Knop, O. Polyhalide Anions in Crystals. 3. The Br_8^{2-}
24 Anion in Diquinuclidinium Octabromide, the Crystal Structures of Me_4PBr_3 and Quinuclidinium Tribromide,
25 and Ab Initio Calculations on Polybromide Anions. *Z. Anorg. Allg. Chem.* **1997**, *623*, 104-114.
26
27
28
29 (15) Evans, J. C.; Lo, G. Y. S. Vibrational Spectra of Cl_3^- Ion and Evidence for Existence of Cl_5^- . *J. Chem.*
30 *Phys.* **1966**, *44*, 3638-3639.
31
32
33 (16) Burns, G. R.; Renner, R. M. A Raman and Resonance Raman Study of Polybromide Anions and a Study
34 of the Temperature Dependence of the Raman-Active Phonons of Tetrabutylammonium Tribromide.
35 *Spectrochim. Acta, Pt. A: Mol. Spectrosc.* **1991**, *47*, 991-999.
36
37
38 (17) Hunt, R. D.; Thompson, C.; Hassanzadeh, P.; Andrews, L. Matrix IR Spectra of the Products from
39 Fluorine Molecule, Chlorine Molecule, and Chlorine Fluoride (ClF) Reactions with Pulsed-Laser Evaporated
40 Uranium Atoms. *Inorg. Chem.* **1994**, *33*, 388-391.
41
42
43 (18) Tuinman, A. A.; Gakh, A. A.; Hinde, R. J.; Compton, R. N. The First Direct Observation of the
44 Trifluoride Anion (F_3^-) in the Gas Phase. *J. Am. Chem. Soc.* **1999**, *121*, 8397-8398.
45
46
47 (19) Artau, A.; Nizzi, K. E.; Hill, B. T.; Sunderlin, L. S.; Wenthold, P. G. Bond Dissociation Energy in
48 Trifluoride Ion. *J. Am. Chem. Soc.* **2000**, *122*, 10667-10670.
49
50
51 (20) Landrum, G. A.; Goldberg, N.; Hoffmann, R. Bonding in the Trihalides (X_3^-), Mixed Trihalides (X_2Y^-)
52 and Hydrogen Bihalides (X_2H^-). The Connection between Hypervalent, Electron-Rich Three-Center,
53 Donor-Acceptor and Strong Hydrogen Bonding. *J. Chem. Soc.-Dalton Trans.* **1997**, 3605-3613.
54
55
56 (21) Munzarova, M. L.; Hoffmann, R. Electron-Rich Three-Center Bonding: Role of s,p Interactions across
57
58
59
60

- 1
2
3 the p-Block. *J. Am. Chem. Soc.* **2002**, *124*, 4787-4795.
- 4
5 (22) Braida, B.; Hiberty, P. C. What Makes the Trifluoride Anion F_3^- So Special? A Breathing-Orbital Valence
6
7 Bond ab Initio Study. *J. Am. Chem. Soc.* **2004**, *126*, 14890-14898.
- 8
9 (23) Braida, B.; Hiberty, P. C. Application of the Valence Bond Mixing Configuration Diagrams to
10
11 Hypervalency in Trihalide Anions: A Challenge to the Rundle-Pimentel Model. *J. Phys. Chem. A* **2008**, *112*,
12
13 13045-13052.
- 14
15 (24) Ciancaleoni, G.; Arca, M.; Caramori, G. F.; Frenking, G.; Schneider, F. S. S.; Lippolis, V. Bonding
16
17 Analysis in Homo- and Hetero-Trihalide Species: A Charge Displacement Study. *Eur. J. Inorg. Chem.* **2016**,
18
19 *2016*, 3804-3812.
- 20
21 (25) Hach, R. J.; Rundle, R. E. The Structure of Tetramethylammonium Pentaiodide. *J. Am. Chem. Soc.* **1951**,
22
23 *73*, 4321-4324.
- 24
25 (26) Pimentel, G. C. The Bonding of Trihalide and Bifluoride Ions by the Molecular Orbital Method. *J. Chem.*
26
27 *Phys.* **1951**, *19*, 446-448.
- 28
29 (27) Heard, G. L.; Marsden, C. J.; Scuseria, G. E. The Trifluoride Anion: A Difficult Challenge for Quantum
30
31 Chemistry. *J. Phys. Chem.* **1992**, *96*, 4359-4366.
- 32
33 (28) Mota, F.; Novoa, J. J. The Symmetry Breaking Problem in the Trifluoride Anion: A Multireference
34
35 Approach. *J. Chem. Phys.* **1996**, *105*, 8777-8784.
- 36
37 (29) Tozer, D. J.; Carlos P, S. The Alkali Metal Trifluorides $M^+F_3^-$: How Well Can Theory Predict Experiment?
38
39 *Mol. Phys.* **1997**, *90*, 515-524.
- 40
41 (30) Getmanskii, I. V.; Koval, V. V.; Minyaev, R. M.; Minkin, V. I. Dependence of the Structure of Alkali
42
43 Metal–Trifluoride Ion Pairs $F_3^- M^+$ on the Counterion M^+ ($M = Li, Na, K$). *Mendeleev Commun.* **2015**, *25*,
44
45 417-419.
- 46
47 (31) Vent-Schmidt, T.; Brosi, F.; Metzger, J.; Schlöder, T.; Wang, X.; Andrews, L.; Müller, C.; Beckers, H.;
48
49 Riedel, S. Fluorine-Rich Fluorides: New Insights into the Chemistry of Polyfluoride Anions. *Angew. Chem.*
50
51 *Int. Ed.* **2015**, *54*, 8279-8283.
- 52
53 (32) Ault, B. S.; Andrews, L. Matrix Reactions of Alkali Metal Fluoride Molecules with Fluorine. Infrared and
54
55 Raman Spectra of the Trifluoride Ion in the $M^+F_3^-$ Species. *J. Am. Chem. Soc.* **1976**, *98*, 1591-1593.
- 56
57 (33) Ault, B. S.; Andrews, L. Infrared and Raman Spectra of the $M^+F_3^-$ Ion Pairs and Their Mixed
58
59 Chlorine-Fluorine Counterparts in Solid Argon. *Inorg. Chem.* **1977**, *16*, 2024-2028.
- 60
61 (34) Vosko, S. H.; Wilk, L.; Nusair, M. Accurate Spin-Dependent Electron Liquid Correlation Energies for

1
2
3 Local Spin Density Calculations: A Critical Analysis. *Can. J. Phys.* **1980**, *58*, 1200-1211.

4
5 (35) Becke, A. D. Density-Functional Exchange-Energy Approximation with Correct Asymptotic Behavior.
6
7 *Phys. Rev. A* **1988**, *38*, 3098-3100.

8
9 (36) Lee, C. T.; Yang, W. T.; Parr, R. G. Development of the Colle-Salvetti Correlation-Energy Formula into a
10
11 Functional of the Electron-Density. *Phys. Rev. B* **1988**, *37*, 785-789.

12
13 (37) Werner, H.-J.; Knowles, P. J.; Knizia, G.; Manby, F. R.; Schütz, M. MOLPRO: A General-Purpose
14
15 Quantum Chemistry Program Package. *Wiley Interdiscip. Rev. Comput. Mol. Sci.* **2012**, *2*, 242-253.

16
17 (38) Werner, H.-J.; Knowles, P. J.; Knizia, G.; Manby, F. R.; Schütz, M.; Celani, P.; Györfy, W.; Kats, D.;
18
19 Korona, T.; Lindh, R. *et al.*, MOLPRO, version 2010.1, a package of *ab initio* programs, **2010**, see
20
21 <http://www.molpro.net>.

22
23 (39) Prascher, B. P.; Woon, D. E.; Peterson, K. A.; Dunning, T. H.; Wilson, A. K. Gaussian Basis Sets for Use
24
25 in Correlated Molecular Calculations. VII. Valence, Core-Valence, and Scalar Relativistic Basis Sets for Li,
26
27 Be, Na, and Mg. *Theor. Chem. Acc.* **2011**, *128*, 69-82.

28
29 (40) Hill, J. G.; Peterson, K. A. Gaussian Basis Sets for Use in Correlated Molecular Calculations. XI.
30
31 Pseudopotential-based and All-electron Relativistic Basis Sets for Alkali Metal (K–Fr) and Alkaline Earth
32
33 (Ca–Ra) Elements. *J. Chem. Phys.* accepted.

34
35 (41) Woon, D. E.; Dunning, T. H. Gaussian Basis Sets for Use in Correlated Molecular Calculations. III. The
36
37 Atoms Aluminum through Argon. *J. Chem. Phys.* **1993**, *98*, 1358-1371.

38
39 (42) Peterson, K. A.; Figgen, D.; Goll, E.; Stoll, H.; Dolg, M. Systematically Convergent Basis Sets with
40
41 Relativistic Pseudopotentials. II. Small-Core Pseudopotentials and Correlation Consistent Basis Sets for the
42
43 Post-*d* Group 16–18 Elements. *J. Chem. Phys.* **2003**, *119*, 11113-11123.

44
45 (43) Raghavachari, K.; Trucks, G. W.; Pople, J. A.; Head-Gordon, M. A Fifth-Order Perturbation Comparison
46
47 of Electron Correlation Theories. *Chem. Phys. Lett.* **1989**, *157*, 479-483.

48
49 (44) Bartlett, R. J.; Watts, J. D.; Kucharski, S. A.; Noga, J. Non-Iterative Fifth-Order Triple and Quadruple
50
51 Excitation Energy Corrections in Correlated Methods. *Chem. Phys. Lett.* **1990**, *165*, 513-522.

52
53 (45) Stanton, J. F. Why CCSD(T) Works: A Different Perspective. *Chem. Phys. Lett.* **1997**, *281*, 130-134.

54
55 (46) Shavitt, I.; Bartlett, R. J., *Many-Body Methods in Chemistry and Physics: MBPT and Coupled-Cluster*
56
57 *Theory* (Cambridge University Press, Cambridge, UK, 2009).

58
59 (47) Harding, M. E.; Metzroth, T.; Gauss, J.; Auer, A. A. Parallel Calculation of CCSD and CCSD(T) Analytic
60
61 First and Second Derivatives. *J. Chem. Theory Comput.* **2008**, *4*, 64-74.

- 1
2
3 (48) CFOUR, a quantum chemical program package by Stanton, J. F.; Gauss, J.; Harding, M. E.; Szalay, P. G.
4 with contributions from Auer, A. A.; Bartlett, R. J.; Benedikt, U.; Berger, C.; Bernholdt, D. E.; Bomble, Y. J.;
5 Cheng, L.; Christiansen, O.; Heckert, M.; Heun, O. *et al.*, and the integral packages *MOLECULE* (Almlöf, J.
6 and Taylor, P. R.), *PROPS* (Taylor, P. R.), *ABACUS* (Helgaker, T.; Jensen, H. J. Aa.; Jørgensen, P.; and Olsen,
7 J.), and ECP routines by Mitin, A. V. and van Wüllen, C. For the current version see, <http://www.cfour.de>.
8
9 (49) Peterson, K. A.; Dunning, T. H. Accurate Correlation Consistent Basis Sets for Molecular Core–Valence
10 Correlation Effects: The Second Row Atoms Al–Ar, and the First Row Atoms B–Ne Revisited. *J. Chem. Phys.*
11 **2002**, *117*, 10548-10560.
12
13 (50) Peterson, K. A.; Shepler, B. C.; Figgien, D.; Stoll, H. On the Spectroscopic and Thermochemical
14 Properties of ClO, BrO, IO, and Their Anions. *J. Phys. Chem. A* **2006**, *110*, 13877-13883.
15
16 (51) Peterson, K. A.; Yousaf, K. E. Molecular Core-Valence Correlation Effects Involving the Post-D
17 Elements Ga–Rn: Benchmarks and New Pseudopotential-Based Correlation Consistent Basis Sets. *J. Chem.*
18 *Phys.* **2010**, *133*, 174116.
19
20 (52) Lim, I. S.; Schwerdtfeger, P.; Metz, B.; Stoll, H. All-Electron and Relativistic Pseudopotential Studies for
21 the Group 1 Element Polarizabilities from K to Element 119. *J. Chem. Phys.* **2005**, *122*, 104103.
22
23 (53) Blaudeau, J. P.; Brozell, S. R.; Matsika, S.; Zhang, Z.; Pitzer, R. M. Atomic Orbital Basis Sets for Use
24 with Effective Core Potentials. *Int. J. Quantum Chem* **2000**, *77*, 516-520.
25
26 (54) Christiansen, P. A. Basis Sets in Correlated Effective Potential Calculations. *J. Chem. Phys.* **2000**, *112*,
27 10070-10074.
28
29 (55) Peterson, K. A. Systematically Convergent Basis Sets with Relativistic Pseudopotentials. I. Correlation
30 Consistent Basis Sets for the Post-*d* Group 13–15 Elements. *J. Chem. Phys.* **2003**, *119*, 11099-11112.
31
32 (56) Glendening, E. D.; Landis, C. R.; Weinhold, F. Natural Bond Orbital Methods. *Wiley Interdiscip. Rev.*
33 *Comput. Mol. Sci.* **2012**, *2*, 1-42.
34
35 (57) Matta, C. F.; Boyd, R. J., in *The Quantum Theory of Atoms in Molecules* (Wiley-VCH Verlag GmbH &
36 Co. KGaA, **2007**), pp. 1-34.
37
38 (58) NBO 6.0. Glendening E. D.; Badenhoop J. K.; Reed A. E.; Carpenter J. E.; Bohmann J. A.; Morales C.
39 M.; Landis C. R.; Weinhold F., Theoretical Chemistry Institute, University of Wisconsin, Madison (**2013**)
40
41 (59) Glendening, E. D.; Badenhoop, J. K.; Weinhold, F. Natural Resonance Theory: III. Chemical
42 Applications. *J. Comput. Chem.* **1998**, *19*, 628-646.
43
44 (60) Glendening, E. D.; Weinhold, F. Natural Resonance Theory: I. General Formalism. *J. Comput. Chem.*
45
46
47
48
49
50
51
52
53
54
55
56
57
58
59
60

1
2
3 **1998**, *19*, 593-609.

4
5 (61) Glendening, E. D.; Weinhold, F. Natural Resonance Theory: II. Natural Bond Order and Valency. *J.*
6 *Comput. Chem.* **1998**, *19*, 610-627.

7
8 (62) Keith T. A., AIMAll (Version 16.01.09), TK Gristmill Software, Overland Park KS, USA, **2016**
9 (aim.tkgristmill.com)

10
11 (63) Linstrom P. J.; Mallard W. G., Eds., NIST Chemistry WebBook, NIST Standard Reference Database
12 Number 69, National Institute of Standards and Technology, Gaithersburg MD, 20899.

13
14 (64) Brückner, R.; Haller, H.; Ellwanger, M.; Riedel, S. Polychloride Monoanions from $[\text{Cl}_3]^-$ to $[\text{Cl}_9]^-$: A
15 Raman Spectroscopic and Quantum Chemical Investigation. *Chem. Eur. J.* **2012**, *18*, 5741-5747.

16
17 (65) Pichierri, F. Structure and Bonding in Polybromide Anions $\text{Br}^-(\text{Br}_2)_n$ ($n=1-6$). *Chem. Phys. Lett.* **2011**,
18 *515*, 116-121.

19
20 (66) Patel, N. N.; Verma, A. K.; Mishra, A. K.; Sunder, M.; Sharma, S. M. The Synthesis of Unconventional
21 Stoichiometric Compounds in the K-Br System at High Pressures. *Phys. Chem. Chem. Phys.* **2017**, *19*,
22 7996-8007.

23
24 (67) Breneman, G. L.; Willett, R. D. The Crystal Structure of Cesium Tribromide and a Comparison of the
25 Br_3^- and I_3^- Systems. *Acta Crystallogr. Sec. B* **1969**, *25*, 1073-1076.

26
27 (68) Tebbe, K. F.; Georgy, U. The Crystal-Structures of Rubidium Triiodide and Thallium Triiodide. *Acta*
28 *Crystallogr. Sect. C-Cryst. Struct. Commun.* **1986**, *42*, 1675-1678.

29
30 (69) Tasman, H. A. CORRECTION. *Acta Crystallogr.* **1955**, *8*, 857-857.

31
32 (70) Tasman, H. A.; Boswijk, K. H. Re-Investigation of the Crystal Structure Of CsI_3 . *Acta Crystallogr.* **1955**,
33 *8*, 59-60.

34
35 (71) Groom, C. R.; Bruno, I. J.; Lightfoot, M. P.; Ward, S. C. The Cambridge Structural Database. *Acta*
36 *Crystallogr. Sect. B: Struct. Sci.* **2016**, *72*, 171-179.

37
38 (72) Svensson, P. H.; Kloo, L. Synthesis, Structure, and Bonding in Polyiodide and Metal Iodide-Iodine
39 Systems. *Chem. Rev.* **2003**, *103*, 1649-1684.

40
41 (73) Runsink, J.; Swen-Walstra, S.; Migchelsen, T. Refinement of the Crystal Structures of $(\text{C}_6\text{H}_5)_4\text{AsI}_3$ and
42 CsI_3 at 20 °C and at -160 °C. *Acta Crystallogr. Sec. B* **1972**, *28*, 1331-1335.

43
44 (74) Wei, S.; Wang, J.; Deng, S.; Zhang, S.; Li, Q. Hypervalent Iodine with Linear Chain at High Pressure.
45 *Sci. Rep.* **2015**, *5*, 14393.

46
47 (75) Havinga, E. E.; Boswijk, K. H.; Wiebenga, E. H. The Crystal Structure of Cs_2I_8 (CsI_4). *Acta Crystallogr.*

1
2
3 **1954**, 7, 487-490.

4
5 (76) Toman, K.; Honzl, J.; Jecny, J. The Crystal Structure of a Polyiodide Complex with *N*-methylacetamide -
6 KI.KI₃.6(CH₃CONHCH₃). *Acta Crystallogr.* **1965**, 18, 673-677.

7
8 (77) Thomas, R.; Moore, F. H. Neutron Diffraction Studies of Polyiodides. I. Potassium Triiodide
9 Monohydrate. *Acta Crystallogr. Sec. B* **1980**, 36, 2869-2873.

10
11 (78) Zhang, W.; Oganov, A. R.; Goncharov, A. F.; Zhu, Q.; Boulfelfel, S. E.; Lyakhov, A. O.; Stavrou, E.;
12 Somayazulu, M.; Prakapenka, V. B.; Konôpková, Z. Unexpected Stable Stoichiometries of Sodium Chlorides.
13
14
15 *Science* **2013**, 342, 1502-1505.

16
17 (79) Jacox, M. E. The Spectroscopy of Molecular Reaction Intermediates Trapped in the Solid Rare Gases.
18
19
20 *Chem. Soc. Rev.* **2002**, 31, 108-115.

21 (80) Vincent, H.; Monteil, Y.; Berthet, M. P. The Thiotriethiazyl Iodated Polyhalides. *J. Inorg. Nucl. Chem.*
22
23 **1980**, 42, 5-7.

24
25 (81) Maki, A. G.; Forneris, R. Infrared and Spectra of Some Trihalide Ions: ICl₂⁻, IBr₂⁻, I₃⁻, I₂Br⁻, and BrICl⁻.
26
27 *Spectrochim. Acta, Pt. A: Mol. Spectrosc.* **1967**, 23, 867-880.

28
29 (82) F. Weinhold and C. R. Landis, Valency and Bonding: A Natural Bond Orbital Donor-Acceptor
30 Perspective (Cambridge University Press, 2005).

31
32 (83) Bader, R. F. W.; Essén, H. The Characterization of Atomic Interactions. *J. Chem. Phys.* **1984**, 80,
33
34 1943-1960.

35
36 (84) Eriksson, S. K.; Josefsson, I.; Ottosson, N.; Öhrwall, G.; Björneholm, O.; Siegbahn, H.; Hagfeldt, A.;
37 Odelius, M.; Rensmo, H. Solvent Dependence of the Electronic Structure of I⁻ and I₃⁻. *J. Phys. Chem. B* **2014**,
38
39 118, 3164-3174.

40
41 (85) Jena, N. K.; Josefsson, I.; Eriksson, S. K.; Hagfeldt, A.; Siegbahn, H.; Björneholm, O.; Rensmo, H.;
42 Odelius, M. Solvent-Dependent Structure of the I₃⁻ Ion Derived from Photoelectron Spectroscopy and Ab
43
44 Initio Molecular Dynamics Simulations. *Chem. Eur. J.* **2015**, 21, 4049-4055.